407 614

HR-63-264

MICROSTRUCTURE AND MECHANICAL PROPERTIES OF CERAMICS

Nineteenth Technical Report

By

R. J. Stokes

Office of Naval Research Project

Nonr-4076(00) NR-032-451

May 1963

HONEYWELL

MICROSTRUCTURE AND MECHANICAL PROPERTIES OF CERAMICS

Nineteenth Technical Report

By

R. J. Stokes

Office of Naval Research Project

Nonr-4076(00) NR-032-451

May 1963

Honeywell Research Center
Hopkins, Minnesota

TABLE OF CONTENTS

		Page
ABSTRACT		
I.	INTRODUCTION	1
II.	ELASTIC DEFORMATION	2
III.	ANELASTIC BEHAVIOR	8
IV.	PLASTIC DEFORMATION	15
	1. Single Crystals	15
	2. Polycrystals	25
V.	BRITTLE FRACTURE	32
	1. Crack Nucleation Due to Slip at Grain Boundaries	33
	2. Effect of Porosity and Grain Size	38
VI.	HIGH TEMPERATURE DEFORMATION AND CREEP	41
	1. Plastic Deformation and Ductile Fracture	41
	2. Creep and High Temperature Fracture	42
VII.	CONCLUSIONS	55
REFERENCES		58

LIST OF ILLUSTRATIONS

Figure		Page
1	The variation in elastic modulus of a two phase solid. Comparison of theoretical and experimental relationships for the system zirconium carbide plus carbon. (After Hasselman and Schaffer[7]).	3
2	Effect of porosity on elastic (E) and shear (S) moduli of polycrystalline magnesia at room temperature. Letters after author names are fabrication codes, H. P. -hot pressed, C. P. -cold pressed and sintered, and S. C. -slip cast and sintered. (After Spriggs et al[15]).	6
3	Change in damping capacity (internal friction) and dynamic elastic modulus with frequency. Amplitude and temperature constant.	9
4	The internal friction spectrum for single crystal and polycrystalline alumina. (After Chang[19]).	11
5	Effect of impurity on the internal friction spectrum of polycrystalline alumina. The addition of 1% SiO_2 introduces a new low temperature internal friction peak. (After Crandall et al[22])	12
6	Effect of plastic deformation on the internal friction spectrum of magnesium oxide single crystals (After Chang[29]).	14
7	"Grown In" Dislocations in Magnesium Oxide. Note the Impurity Precipitate Particles Spaced at Fairly Regular Intervals. (Electron Transmission Micrograph. Courtesy of G. W. Groves)	20

LIST OF ILLUSTRATIONS (Continued)

Figure		Page
8	Solid solution and precipitation hardening in the silver chloride-sodium chloride alloy system.	22
9	Effect of heat treatment on the room temperature yield strength of commercial purity magnesium oxide single crystals.	24
10	Tensile stress-strain curves for polycrystalline sodium chloride at room temperature illustrating the effect of decreasing the grain size on the proportional limit and rate of work hardening.	28
11	Slip distribution in the vicinity of grain boundaries in lithium fluoride deformed at room temperature. Note very local slip on $\{001\}$ planes near triple point. Slip revealed by etch pit techniques. (Courtesy W. D. Scott and J. A. Pask).	29
12	Nucleation of a cleavage crack due to dislocation pile up at a grain boundary. Magnesium oxide bi-crystal deformed in compression. Slip revealed by etch pit technique.	
13	Effect of purity on the steady state creep rate of alumina. The addition of 2% Cr_2O_3 lowers the creep rate by $\sim 10^4$. (After Chang[101]).	48
14	Comparison of the diffusion coefficient measured for self diffusion of the aluminum ion with the diffusion coefficient calculated from creep data of alumina using the Nabarro-Herring equation. (After Paladino and Coble[105]).	49

LIST OF ILLUSTRATIONS (Continued)

Figure		Page
15	Generation of intergranular voids during torsional creep of high density alumina (courtesy R. L. Coble).	52
16	Effect of porosity on the torsional creep of sintered alumina at 1275° C. The stress to promote a constant creep rate and the creep rate at a constant stress are both plotted as a function of the porosity. (After Coble and Kingery [109]).	53

LIST OF TABLES

Table		Page
1	The number of independent slip systems for some common ceramic crystal structures.	26
2	Tensile strength of magnesium oxide in the absence and presence of "Fresh" surface dislocations.	37
3	Comparison of torsional creep rate for different polycrystalline ceramic materials.	45
4	High temperature deformation and creep of single and polycrystalline alumina.	46

ABSTRACT

In this review paper* the influence of microstructure on the following aspects of mechanical behavior has been considered, (1) elastic deformation, (2) anelastic behavior, (3) plastic deformation, (4) brittle fracture, (5) high temperature deformation and creep. In addition to familiar variables such as grain size and the presence and distribution of porosity or a second phase, the term microstructure has been considered broadly enough to allow discussion of the role that fundamental variables such as crystal structure, bond character and crystalline defects, impurities, vacancies and dislocations play in determining mechanical behavior.

---

*Paper presented at Ceramic Educational Council Seminar, "Microstructure of Ceramic Materials", 65th Annual Meeting American Ceramic Society, Pittsburg, April 27-28, 1963.

I. INTRODUCTION

The last review article on this subject was prepared by Coble in 1956 and was subsequently published in 1958[1]. Since that time, a number of conferences on allied topics have been held and the proceedings published but no review specifically on the effects of microstructure has appeared. The period 1956 to the present has been particularly productive since it corresponded at the start with the beautiful etching experiments on dislocations in lithium fluoride by Gilman and Johnston[2] and the demonstration by Gorum et al[3] that single crystals of magnesium oxide could be deformed plastically at room temperature. The implication from this latter work, that certain ceramic materials might possess ductility, led to increased research activity in the field of the mechanical behavior of ceramics. Most of the early effort concentrated on the behavior of dislocations in single crystals of a relatively few substances, particularly those having the cubic rock salt structure. More recently the field has broadened considerably to include a wider range of single crystal ceramic materials and the earlier work on the rock salt structure has been extended to include the effects of microstructure.

In this paper the influence of microstructure on the following aspects of mechanical behavior will be considered in turn, (1) elastic deformation, (2) anelastic behavior (3) plastic deformation, (4) brittle fracture, (5) high temperature deformation and creep. In addition to the familiar variables such as grain size and the presence and distribution of porosity or a second phase, the term microstructure will be considered broadly enough to allow discussion of the role that fundamental variables such as crystal structure, bond character and crystalline defects such as impurities, vacancies and dislocations play in determining mechanical behavior. By necessity the paper is concerned almost exculsively with the simple oxide ceramics since these materials have been the most extensively studied.

II. ELASTIC DEFORMATION

Purely elastic deformation of a single crystal corresponds to the variation in spacing between atoms under stress. Thus, elastic extension is directly related to the forces between atoms and the binding energy of the structure. Similarly the elastic modulus, the ratio of stress to the extension it produces, is related to bond strength and character. A simple way in which this correlation may be appreciated is to consider the elastic moduli of a number of materials as a function of their melting temperature, the points all fall within a fairly narrow band for which the elastic modulus increases as the melting point increases[4]. Materials of similar type and structure fall into a much narrower band.

The principal effects of microstructure on elastic modulus arise through the presence of a second phase. There are a considerable number of theoretical analyses relating the elastic modulus of heterogeneous systems to the amount of second phase. Each calculation leads to a slightly different relationship enjoying a different degree of success in describing the experimental results. In the simplest case, where the bond between the matrix (the continuous phase) and the inclusions remains continuous and the two phases have the same value for Poisson's ratio, the resultant modulus (E) is given by the simple relationship:

$$E = E_o(1-c) + E_1 c.$$

or

$$E = E_o - c\,(E_o - E_1) \qquad (1)$$

where E_o is the modulus for the matrix, E_1 is the modulus for the included second phase and c is the volume fraction of the second phase. This gives a linear relationship between the modulus of the two end components as indicated in Figure 1.

In general the elastic modulus of a two-phase solid does not vary linearly and the value is always less than that predicted by the linear relationship. Probably the

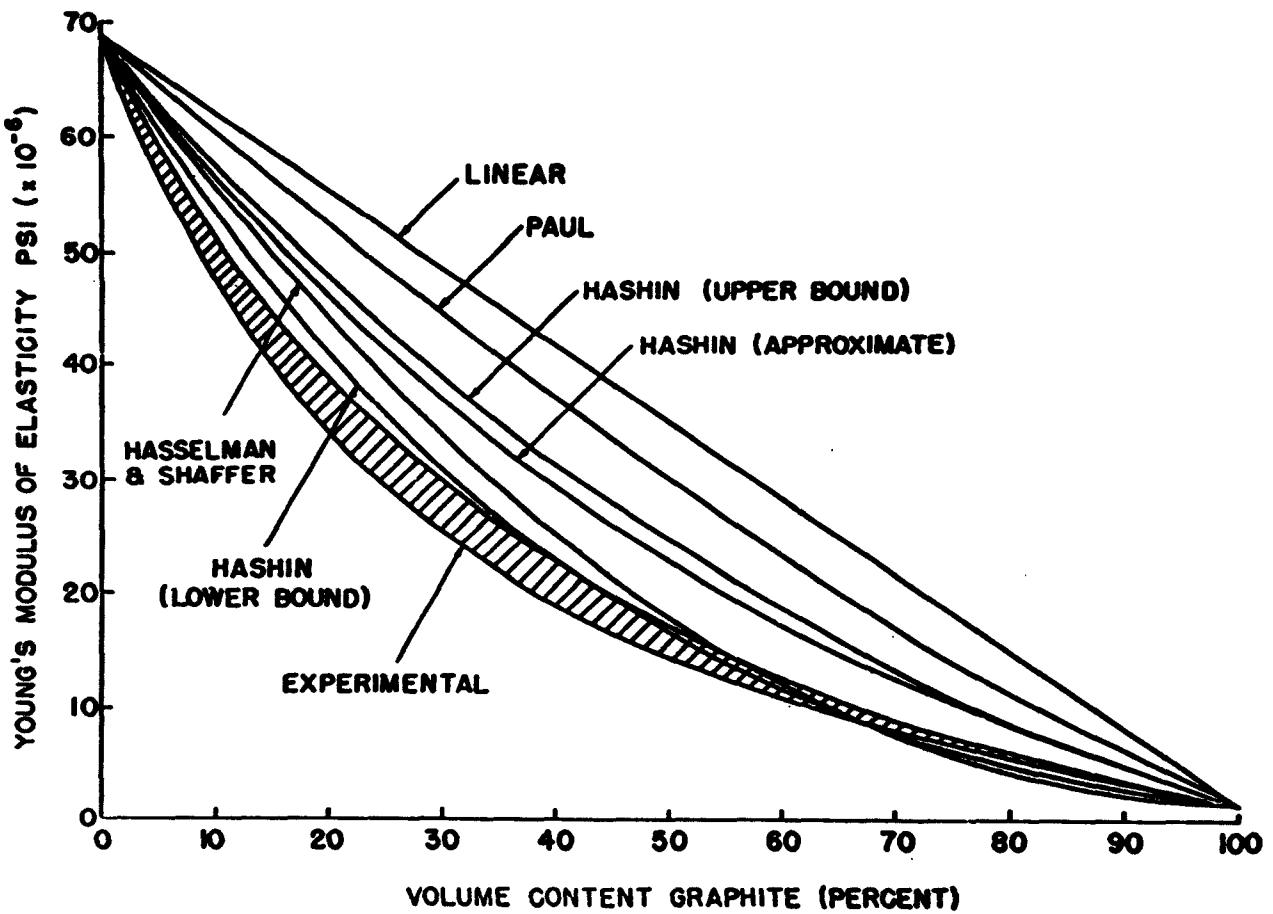

Figure 1 - The variation in elastic modulus of a two phase solid. Comparison of theoretical and experimental relationships for the system zirconium carbide plus carbon. (After Hasselman and Shaffer[7])

most successful analyses for predicting the modulus of heterogeneous solids are the recent ones by Paul[5] and Hashin[6] and the modification to Hashin's analysis by Hasselman and Shaffer[7]. These authors consider the more general case where values for Poisson's ratio of the two phases are not the same and examine the influence of particle shape. Both Paul[5] and Hashin[6] used the system tungsten carbide-cobalt, investigated by Nishimatsui and Gurland[8] and others, for verification of their equations, obtaining good agreement with experiment. In later work, Hasselman and Shaffer[7] and Hasselman[9] applied these equations to their measurement of the variation of elastic modulus for zirconium carbide containing graphite. These results are reproduced in Figure 1, where it appears that Hashin's equation, in particular the lower boundary, shows the best agreement. The equations for shear or bulk modulus derived by Hashin[6] can be written in the general form:

$$E = E_o - c\,(E_o - E_1)\,\frac{A\,E_o}{E_o + B\,\left[E_1 + (E_o - E_1)\,c\right]} \qquad (2)$$

where $A = B + 1$ is a numerical constant.

For the case where the second phase is porosity, i.e., $E_1 = 0$, equation (2) reduces to

$$E = E_o\left[1 - \frac{PA}{1+BP}\right] \qquad (3)$$

where P is the porosity. Other simplified theoretical relationships for the dependence of modulus on porosity are

$$E = E_o\left[1 - 1.9P + 0.9P^2\right] \qquad (4)$$

when ν (Poisson's ratio) = 0.3 derived by MacKenzie [10] for an elastic solid containing spherical holes and

$$E = E_o \left[\frac{1 - P^{2/3}}{1 + P - P^{2/3}} \right] \tag{5}$$

derived by Paul[5] for a solid containing holes of cubic shape. Pores of both shapes can be seen in a ceramic body depending upon their location and the crystal structure. The equation due to MacKenzie has been applied by Coble and Kingery[11] to their measurements on sintered alumina with excellent agreement.

In addition, the relationship:

$$E = E_o e^{-kp} \tag{6}$$

where k is a numerical constant, has been devised on a purely empirical basis by Murray et al[12], to describe experimental results on the effect of porosity on the modulus of beryllium oxide. A similar relationship for alumina was suggested by Spriggs[13], and investigated by Knudsen[14] who accumulated all the available data on this material and showed that the exponential relationship gave a very adequate representation out to 40% porosity with k = 4. Spriggs et al[15] have also used it for magnesia containing up to 25% porosity; their results are reproduced in Figure 2. Use of the empirical exponential relationship in equation (6) has been criticized by Hasselmann[16] on the grounds that it does not have any fundamental basis and does not satisfy the boundary condition E = 0 when P = 1, he suggests that equation (3) due to Hashin[6] can be used with equal success and is more flexible.

In fact the exponential function when expanded takes on a form similar to equation (4) apart from the numerical factor which depends on k. All of the equations (3) through (6) give a fairly adequate representation of the modulus dependence on porosity and it is difficult to make a critical choice between them. Obviously the microstructural variables from specimen to specimen make it virtually impossible to define a practical ceramic in terms of a mathematical model. It is highly probable that the size, shape and location of the pores as well as the total porosity governs the success of any particular equation.

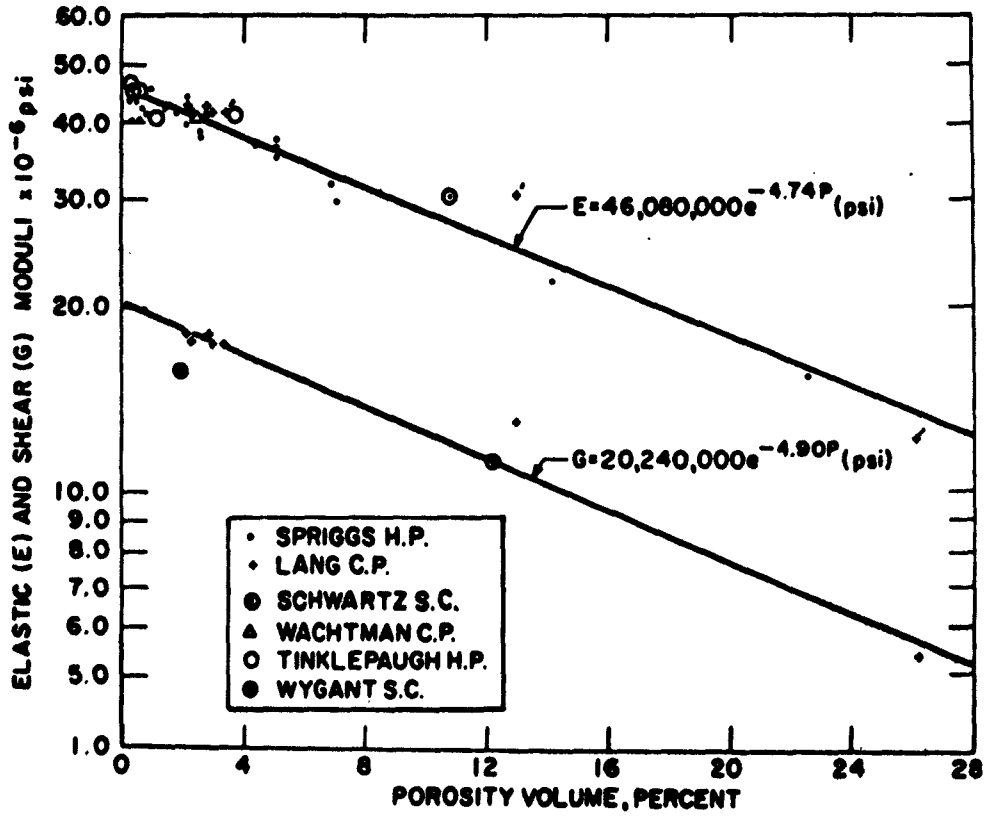

Figure 2 - Effect of porosity on elastic (E) and shear (S) moduli of polycrystalline magnesia at room temperature. Letters after author names are fabrication codes, H. P. - hot pressed, C. P. - cold pressed and sintered, and S. C. - slip cast and sintered. (After Spriggs et al[15])

Other microstructural parameters such as grain size or texture have little or no effect on the elastic modulus. In their studies on alumina and magnesia, Spriggs and Vasilos [17] found the dynamic modulus to be relatively insensitive to variations in grain size for specimens having the same porosity. Although no specific studies have been made, the major effects of texture (alignment of the grains in an extruded body for example) are to be expected in those materials of non-cubic crystal structure possessing strongly anisotropic elastic constants.

In conclusion, it may be stated that for purposes of mechanical strength and rigidity the maximum elastic modulus is generally desirable and this is obtained in material of the highest density, in structures where the solid phase is continuous and the pores are closed and spherical.

III. ANELASTIC BEHAVIOR

When a stress is applied to a body in the elastic region it does not necessarily come to equilibrium immediately but approaches the total strain value asymptotically with time. This so-called "anelastic" effect[18] becomes particularly important when a periodic stress is applied since the resulting hysteresis loop causes energy to be dissipated by the solid.

The magnitude of the energy dissipated at a particular temperature, generally referred to as the internal friction, depends on the strain amplitude and frequency of the imposed vibrations. With the amplitude constant, the internal friction goes through a maximum when the frequency is varied, as shown in Figure 3. The time interval at this critical frequency corresponds to the relaxation time for the particular process responsible for the peak. At the same frequency, the dynamic elastic modulus changes discontinuously, increasing as the frequency is raised through the critical range because the relaxation process then has insufficient time to contribute to the "elastic" strain. This is also illustrated in Figure 3. For experimental purposes it is generally more convenient to use the natural frequency of a specimen and to vary its temperature. In this case the internal friction goes through a peak at a characteristic temperature and there is usually an accompanying inflexion in the dynamic modulus versus temperature curve. By studying the displacement of the peak along the temperature scale for different specimen frequencies it is possible to estimate the activation energy for the relaxation process.

Studies of the internal friction spectrum as a function of temperature, strain amplitude and microstructure have provided powerful research tools for understanding the internal structure and atomic movements in solids. But internal friction is also important from a practical viewpoint in that it constitutes the damping capacity of a freely vibrating solid; depending on the particular application, one may desire either a very high or a very low rate of damping. In the remainder of this section we will review briefly the effect of microstructure on the internal friction, or damping capacity, of ceramics.

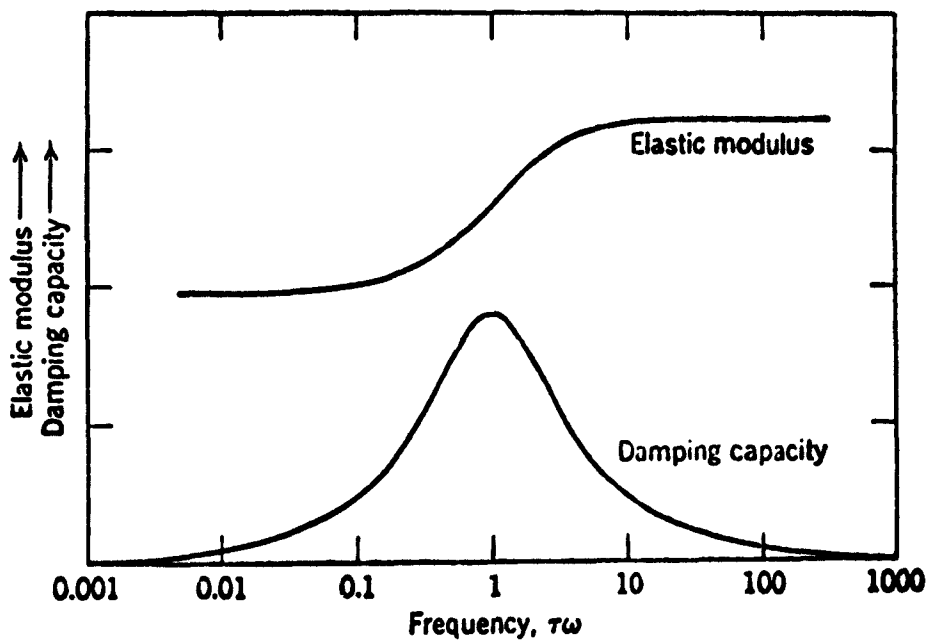

Figure 3 - Change in damping capacity (internal friction) and dynamic elastic modulus with frequency. Amplitude and temperature constant.

The most important microstructural effect is that associated with the presence of grain boundaries. Figure 4 due to Chang[19] shows the difference in internal friction between monocrystalline and polycrystalline alumina as a function of temperature. The internal friction peak at 1100° C is observed only in the polycrystalline material and has been attributed to grain boundary sliding by Wachtman and Maxwell[20] and Chang[19]. Correspondingly Wachtman and Maxwell[20] have shown that the dynamic elastic modulus drops off in value very rapidly at this temperature due also to integranular relaxation. By measuring the shift in the peak for different frequencies, Chang[19] was able to measure the activation energy for this relaxation process. The value, 200 K cals/mole agreed fairly well with other measurements obtained from creep studies (see later) and the activation energy for self-diffusion of aluminum or oxygen ions in alumina. The implication was that the internal friction peak corresponded to diffusion controlled grain boundary sliding.

The grain boundary relaxation peak in alumina has been the subject of extensive investigation, particularly into the effect of purity. Conventional alumina shows the peak around 1100° C, but for high purity alumina it has been reported as high as 1400° C[21]. The deliberate addition of impurity lowers considerably the temperature of the internal friction peak at a given frequency. Figure 5, taken from the work of Crandall et al[22], shows how the addition of just 1% SiO_2 introduces a new peak around 700° C. Similarly, the addition of small amounts of Cr_2O_3 or La_2O_3 result in the appearance of internal friction peaks at lower temperatures[19, 23]. Also, the addition of 1% MgO has been shown to increase the damping capacity of beryllium oxide at low temperatures[23]. The general interpretation is that impurities tend to enhance grain boundary sliding in ceramic materials, a phenomenon the opposite to that normally observed in metals. The reason for the lower viscosity is not fully understood, it may be assciated with the precipitation of a complex or glassy phase in the grain boundaries or it may be associated with the introduction of a non-equilibrium concentration of vacancies necessary to maintain electrical neutrality when impurity ions of a different valence are added. Obviously, the damping capacity of ceramics at low temperature is exceedingly sensitive to purity.

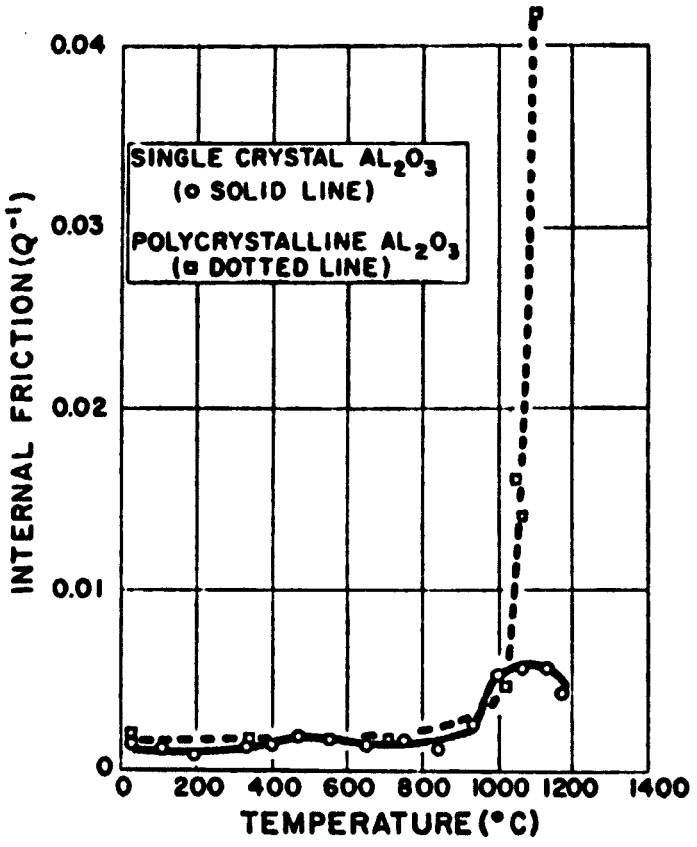

Figure 4 - The internal friction spectrum for single crystal and polycrystalline alumina. (After Chang[19]).

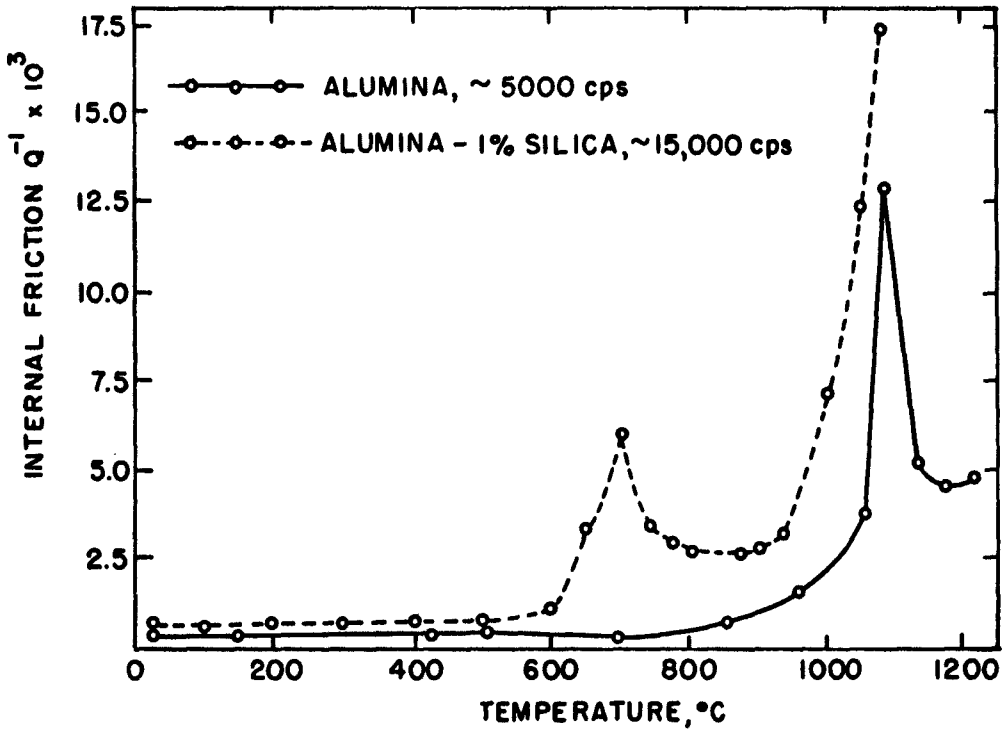

Figure 5 - Effect of impurity on the internal friction spectrum of polycrystalline alumina. The addition of 1% SiO_2 introduces a new low temperature internal friction peak. (After Crandall et al[22]).

Other microstructural features are known to be responsible for internal friction peaks in solids. These include, stress induced phase transformations, stress induced ordering, and relaxation phenomena associated with the presence of incoherent interfaces (inclusions) and the motion of twin interfaces[24]. While these processes have been studied extensively in metallic solids there has been little research in this area on ceramic systems. Chang [23] has suggested that an internal friction peak observed in zirconium hydride around 100° C may be due to twin interface motion.

Another microstructural effect on internal friction at low temperatures is that associated with defects introduced by plastic deformation. Again this is a field which has been investigated primarily in metals[24] and internal friction peaks due to dislocation motion (the so-called Bordoni peak) have been identified. Of the ceramic materials, sodium chloride has been studied in most detail[25, 26], although a limited amount of work has been done on lithium fluoride[27], magnesia[28, 29], and alumina[29]. In general the damping increases with the amount of plastic deformation and is observed so long as the dislocations are mobile. Thus procedures to lock dislocations by heat treatment or X-irradiation[25] result in a decrease in the damping capacity. The effect of plastic deformation on the internal friction spectrum of magnesium oxide is illustrated in Figure 6. In this material plastic deformation enhances the damping capacity around room temperature. The equivalent dislocation damping peak is not observed in alumina until around 1500° C and, as Chang[29] has pointed out, this difference in behavior is a reflection of the relative dislocation mobility in these two solids (see later). In this respect the damping capacity of a single crystal at a certain temperature is influenced by its crystal structure, and by the same token the damping capacity may be regarded as a useful indicator as to whether dislocations are mobile in a particular solid at a given temperature or not.

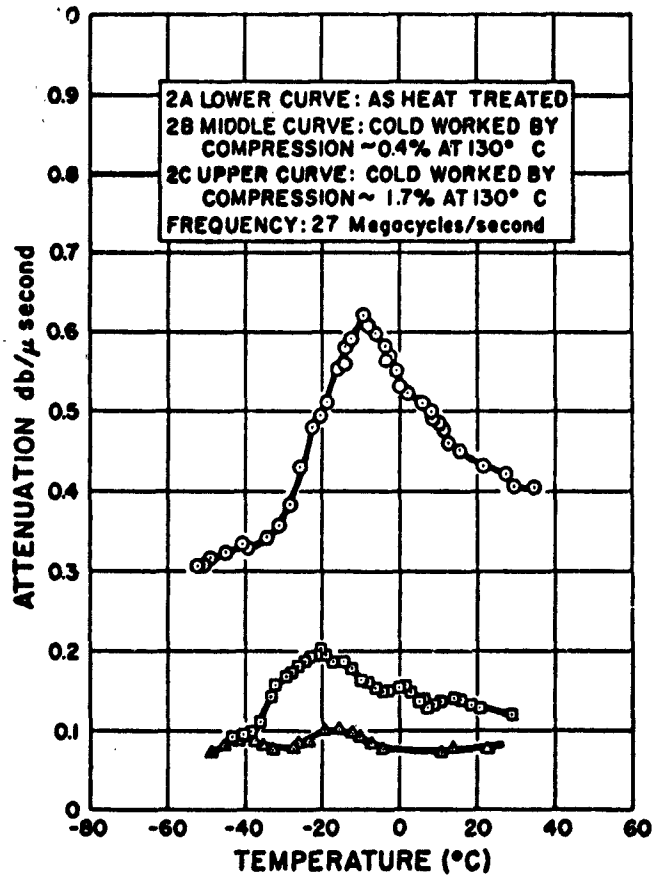

Figure 6 - Effect of plastic deformation on the internal friction spectrum of magnesium oxide single crystals. (After Chang[29]).

IV. PLASTIC DEFORMATION

Plastic deformation in crystalline solids at low temperatures (i.e. $< 0.5T_m$) is due to the generation, motion, and multiplication of dislocations. The previous seminar in this series[30] dealt with some of the more sophisticated aspects of dislocation theory and dislocation interactions in crystalline solids. However, it is important to emphasize here that the properties of dislocations in ceramics are quite different from those in metals. The reasons for this are the short range nature of the bonding forces, the presence of two or more ion species of different size and a more complicated crystal structure. Furthermore, the behavior of dislocations differs from one ceramic material to another and it is dangerous to generalize between them. In this section we shall be concerned with the influence of structural and microstructural elements on the availability and mobility of dislocations and thus on the plastic properties of ceramic materials.

1. Single Crystals

a) Crystal Structure and Bond Character - A dislocation line represents the boundary line between slipped and unslipped portions of a crystal plane. The direction in which slip occurs and the plane selected depend on crystallographic factors, the primary factor being that the slip (or Burgers) vector should correspond to the shortest displacement resulting in crystalline identity. The slip plane is generally the closest packed plane. However, in purely ionic solids there is the additional restriction that displacement should occur in a direction or over a plane which does not cause like ions to be forced into juxtaposition at any stage of the displacement. It is for this reason that magnesium oxide slips in the $[1\bar{1}0]$ direction over $\{110\}$ planes rather than the more densely packed $\{001\}$ planes[31]. For similar reasons the slip direction of cesium chloride type crystals changes from $[111]$ to $[100]$ as the bonding changes from metallic to ionic in nature[32]. Thus bond character is important in determining the slip elements.

Crystal structure also plays a very important role in determining the dislocation configuration, in general the more complex the crystal structure, the more complex the dislocation configuration. Consider alumina for example, the shortest direction of crystalline identity is a $[1\bar{1}20]$, but as Kronberg[33] has shown, it is energetically favorable for this displacement to be achieved in a series of four shorter displacements where the ions ride through the saddle points in the structure. The passage of one of these shorter displacements, or partial dislocations, results in the formation of a planar stacking fault. Thus, dislocations in alumina should consist of four partial dislocations linked by three stacking fault layers. Dislocations in the basal plane of the layer silicates similarly dissociate into four partials and this has been observed directly in talc by the electron transmission technique[34, 35]. Stacking faults linking partial dislocations have been observed directly in a number of other layer structures[34, 35], and in rutile[36]. In magnesium oxide the structure is relatively simple and the dislocations can be thought of as being made by the insertion of two supplementary $\{110\}$ surfaces of positive and negative ions. The two surfaces are necessary to maintain charge balance and they must remain adjacent to maintain continuity. Any tendency for them to dissociate would force like ions into juxtaposition and consequently form a very high energy stacking fault.

The combined influences of bond character and crystal structure have their greatest effect on the relative mobility of dislocations in various ceramic materials. When a dislocation moves, bonds, ionic and covalent, must be broken and remade and in the case of dissociated dislocations the partials must also be moved along together. While the breaking of bonds due to the movement of dislocations is a relatively low energy process in metals, in covalent solids it can be very high. The situation is further complicated in alumina, for example, by the fact that when the dislocation moves, the aluminum ions and oxygen ions in the dislocation core must move in different directions, referred to by Kronberg[33] as "synchro-shear". Only at high

temperatures where ion mobility is high and the motions easy to synchronize can dislocations move easily in alumina. It is for this reason that it is necessary to go to extremely high stresses or high temperatures[37, 38, 39] (greater than 1000° C) to observe plastic deformation in single crystals of this material. It also explains the strong temperature dependence of the yield strength of alumina[39]. In the case of rutile the movement of dislocations requires the rupture of predominantly covalent bonds and this probably explains the inability of this material to deform plastically below 600° C[36]. By contrast the predominantly ionic nature of the bond and the relative simplicity of the dislocation configuration in magnesium oxide makes it possible to deform this material even at liquid nitrogen temperature.

As mentioned earlier, the difference in dislocation mobility between alumina and magnesia is reflected by their relative damping capacity[29], it is also responsible for many of the other contrasting features of their mechanical behavior as we shall discuss in the following sections. Similarly, the effects of microstructure on the mechanical properties of other ceramic materials at a given temperature are conditioned by the relative ease with which dislocations can move.

It is important to realize that the conventional yield strength of a solid corrresponds to a stress level at which large numbers of dislocations are moving with quite a high velocity. The plastic strain rate of a crystal may be written as:

$$\dot{\epsilon} = n b v \qquad (7)$$

where n is the number of mobile dislocations per unit area, a factor which increases rapidly due to dislocation multiplication[40]; b is the Burgers vector; v is the average velocity of the dislocations, a factor which is very sensitive to the local stress. Direct measurements of the velocity-stress dependence by Johnston and Gilman[41] have shown that the velocity of dislocations in lithium fluoride increases approximately as the twenty-fifth power of the stress.

Macroscopic yielding occurs when $\dot{\epsilon}$ (equation (7)) is approximately equal to the imposed strain rate of the testing machine. With sensitive techniques however, it is possible to detect plastic deformation well below the conventional yield strength in the so-called microstrain region. In particular etch pit techniques[42] can be used to measure the stress required to get dislocations moving, this stress is defined as the microscopic yield stress.

Thus, to summarize, the plastic properties of a solid depend critically upon the number of dislocation sources (n) and the mobility of dislocations (v). Dislocation mobility is influenced fundamentally by bond character and crystal structure. All of these parameters must be borne in mind when considering the extra effects due to microstructure.

b) Solid Solution and Precipitation Hardening - First, we discuss the effects due to impurities. Impurities can be present either in solid solution or in the form of precipitate particles and can act in two main ways to change the plastic properties of a crystal. First, they can lock dislocations in place, preventing them from participating in plastic flow and thus reducing the initial value of n in equation (7); and second, they can impede the motion of dislocations through the crystal lattice and thus reduce v in equation (7). Either way the crystal increases in strength.

The most direct example of dislocation locking by impurity is that demonstrated by Stokes [43] on magnesium oxide single crystals. He showed that crystals specially treated to contain only "aged" or "grown in" dislocations supported stresses as high as 140,000 psi. in a purely elastic manner without yielding. In this case all of the dislocations were immobilized and n in equation (7) was zero at all stress levels. On the other hand crystals containing "fresh" dislocations (i.e., dislocations generated at the surface at room temperature and therefore free from any contamination by impurity) deformed plastically at a

Macroscopic yielding occurs when $\dot{\epsilon}$ (equation (7)) is approximately equal to the imposed strain rate of the testing machine. With sensitive techniques however, it is possible to detect plastic deformation well below the conventional yield strength in the so-called microstrain region. In particular etch pit techniques[42] can be used to measure the stress required to get dislocations moving, this stress is defined as the microscopic yield stress.

Thus, to summarize, the plastic properties of a solid depend critically upon the number of dislocation sources (n) and the mobility of dislocations (v). Dislocation mobility is influenced fundamentally by bond character and crystal structure. All of these parameters must be borne in mind when considering the extra effects due to microstructure.

b) Solid Solution and Precipitation Hardening - First, we discuss the effects due to impurities. Impurities can be present either in solid solution or in the form of precipitate particles and can act in two main ways to change the plastic properties of a crystal. First, they can lock dislocations in place, preventing them from participating in plastic flow and thus reducing the initial value of n in equation (7); and second, they can impede the motion of dislocations through the crystal lattice and thus reduce v in equation (7). Either way the crystal increases in strength.

The most direct example of dislocation locking by impurity is that demonstrated by Stokes [43] on magnesium oxide single crystals. He showed that crystals specially treated to contain only "aged" or "grown in" dislocations supported stresses as high as 140,000 psi. in a purely elastic manner without yielding. In this case all of the dislocations were immobilized and n in equation (7) was zero at all stress levels. On the other hand crystals containing "fresh" dislocations (i.e., dislocations generated at the surface at room temperature and therefore free from any contamination by impurity) deformed plastically at a

yield stress of approximately 10,000 psi. The "fresh" dislocations could move and multiply fast enough at this stress level for the plastic strain rate ($\dot{\epsilon}$) to keep up with the testing machine. Similar differences in mechanical behavior between crystals containing "fresh" and "aged" dislocations, although on a less spectacular scale, have been noted in lithium fluoride by Gilman and Johnston[2].

"Grown in" dislocations in magnesium oxide have been observed directly by the electron transmission technique and are found to have precipitate particles strung all along their length[44] as illustrated in Figure 7. The particles have been identified as zirconium dioxide[45], although considering the purity of the crystals there are likely to be other oxides precipitated on the dislocations too. The mechanism by which these particles lock the dislocations is not entirely understood, but it probably involves an elastic interaction between the impurity ions and the stress field of the dislocations.

One of the characteristic features of impurity locking is that it represents a metastable condition. As soon as a single dislocation escapes from its impurity environment it can move and multiply rapidly and the stress level needed to sustain the imposed strain rate falls. Such catastrophic drops in strength at the onset of yielding have been observed in magnesium oxide[43].

The great difference in mechanical behavior between these two conditions (the "presence" or "absence" of "fresh" dislocations) in magnesium oxide has proved to be extremely useful in understanding the origin of brittle fracture in polycrystalline material. We shall return to this point later in connection with Table 2.

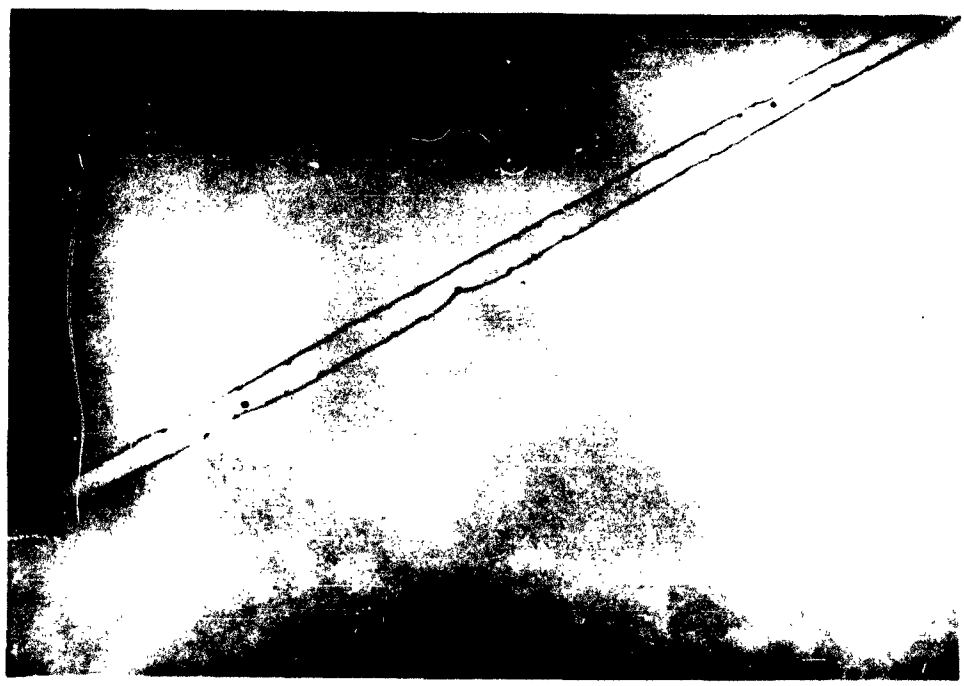

Figure 7 - "Grown In" Dislocations in Magnesium Oxide. Note the Impurity Precipitate Particles Spaced at Fairly Regular Intervals. (Electron Transmission Micrograph Courtesy G. W. Groves).

It is now generally agreed that the permanent strengthening associated with impurities must arise from an increased resistance to dislocation motion through the lattice, i.e., by decreasing the velocity v for a given stress[46]. Local fluctuations in the internal stress field due to the presence of impurity ions impede the dislocations and cause the strengthening. Although the exact differences between solid solution and precipitation hardening are by no means well understood, the stresses due to a coherent precipitate are generally regarded as a much more effective impediment than those due to impurities in solid solution. However, the situation is further complicated in ionic solids by the requirement that electrical neutrality must be maintained at all times and the valency of impurity ions going into solid solution must be taken into consideration. There are, therefore, at least three conditions to be considered, (i) simple solid solution with ions of the same valency, (ii) simple solid solution with ions of different valency, (iii) precipitation.

When the valency of the added impurity ion is the same as that of the ion it is replacing, simple solid solution strengthening is observed. This has been observed in silver chloride, for example, hardened by the addition of silver bromide[47] and in potassium chloride hardened by the addition of potassium bromide[48]. The stress strain characteristics of silver chloride-sodium chloride alloys[49] are compared with the phase diagram in Figure 8 and simple solid solution strengthening is observed at the two extreme ends (i.e., up to 10 mole percent and above 85 mole percent sodium chloride) of the composition scale.

When the valency of the added impurity ion going into solution is different from the ion it is replacing, then an equivalent number of vacancies must be introduced into the host lattice to maintain electrical neutrality. This condition has a remarkable strengthening effect. The influence of divalent alloying elements on the mechanical properties of sodium chloride was studied extensively in Germany in the early 1930's and this work is reviewed in the book by Schmid

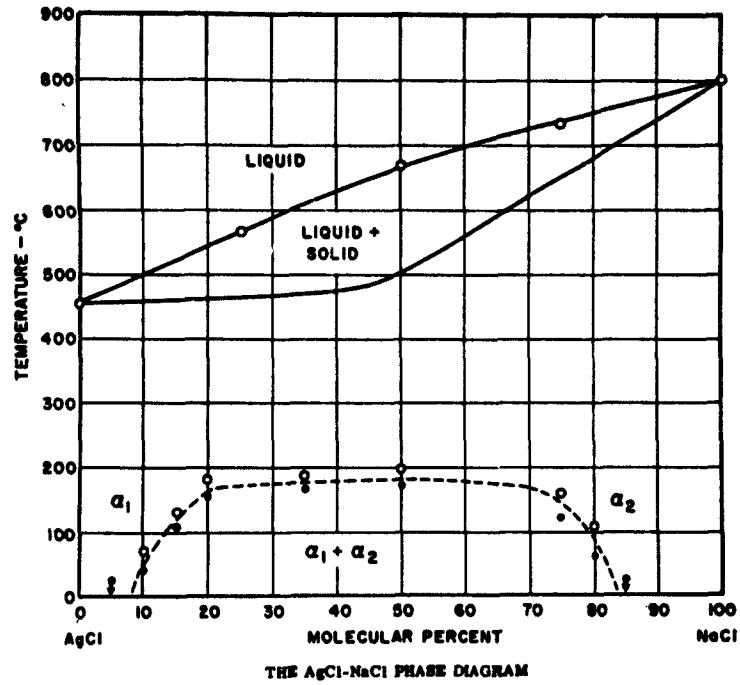

(a)

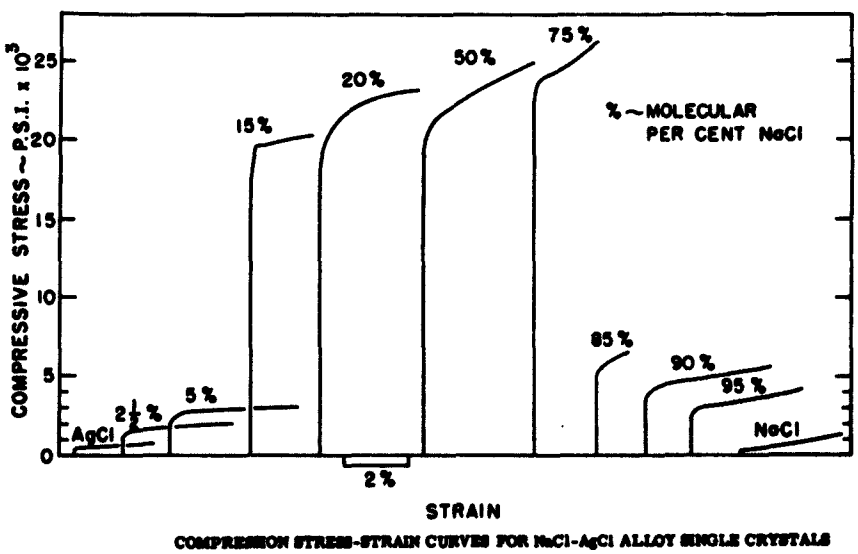

(b)

Figure 8 - Solid solution and precipitation hardening in the silver chloride-sodium chloride alloy system.

and Boas[50]. While the solubility of divalent cations is very restricted, marked hardening is observed for additions in the range 10^{-6} to 10^{-4} mole fractions. Thus, 0.02% calcium chloride in sodium chloride raises the strength fivefold. Similarly, the addition of minute quantities of magnesium fluoride to lithium fluoride result in a tenfold increase in strength[51]. Eshelby et al[52] have proposed a mechanism to account for this strengthening in which they take into consideration the electrostatic attraction between charged dislocations and the charged vacancies, so that the dislocation lines become surrounded by a vacancy cloud which restricts their motion. Other evidence concerning the role of vacancies and point defects in the strengthening of ionic solids is reviewed in the paper by Pratt[53].

There are very few clear cut examples of precipitation hardening in ceramic systems. The best example to date is that observed in the middle composition range of the sodium chloride-silver chloride system illustrated in Figure 8. Sodium chloride-silver chloride alloys show a miscibility gap between 10% and 80% sodium chloride at room temperature and in this same range the strength increases by 50 to 100-fold over that of the end components[49]. However, even in this system the rules of precipitation hardening are not strictly followed in that solution heat-treated crystals are equally as strong as fully precipitated crystals, and it is not certain whether internal stresses due to co-precipitation of the two equilibrium phases are the true source of hardening or not.

As a result of their studies on the effect of heat treatment and temperature on the strength of commercial magnesium oxide crystals, Gorum et al[54], May and Kronberg[55] and Stokes[56] concluded that a precipitation hardening type of mechanism was occurring. Crystals in the as-received (fully precipitated) condition containing many "fresh" dislocation sources were approximately twice as strong as those annealed above 1200° C, as shown in Figure 9 curve A; however,

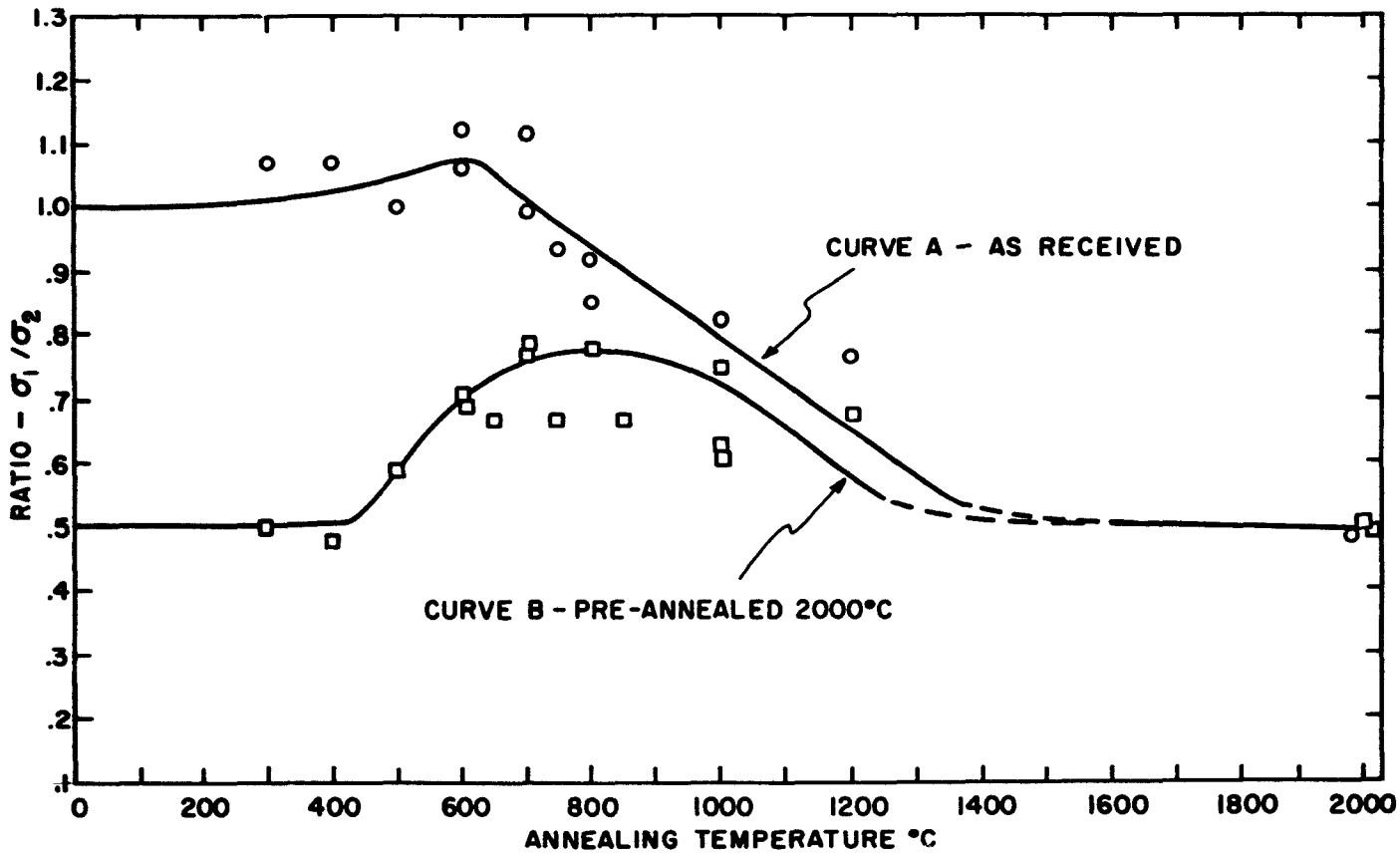

Figure 9 - Effect of heat treatment on the room temperature yield strength of commercial purity magnesium oxide single crystals.
σ_1 - room temperature yield strength in as-received (fully precipitated) condition.
σ_2 - room temperature yield strength after annealing.

the higher strength could be restored by a subsequent anneal around 800° C, Figure 9 curve B. Presumably the anneal above 1200° C dissolved the precipitate particles initially present into solid solution making it easier for the dislocations to move at room temperature. The subsequent anneal at 800° C forced them to reprecipitate again. Unfortunately, this work is currently lacking direct experimental evidence concerning the nature and distribution of the second phase.

Deliberate alloying of magnesium oxide single crystals with small quantities of impurity can lead to remarkable changes in strength, although the strengthening mechanism, i.e., whether due to solid solution, precipitation or point defect hardening has not yet been identified. Saikiewicz[57] showed that single crystals doped with 0.5% Cr_2O_3 raised the compressive strength fivefold to 80,000 psi, a value which dropped by one-half on subsequent vacuum annealing. Liu et al[58] have found a similar strength (80,000 psi) for magnesia containing a few mole percent of MnO, and a strength of 40,000 psi for alloys containing only five mole percent NiO. In the latter case microscopic studies indicate that the nickel ions are in solid solution. There is a need for further work in this area with emphasis on the control of stoichiometry, and the manipulation of microstructure through heat treatment based on complete phase diagrams.

2. Polycrystals

Next, we consider the effect of grain boundaries on the plastic deformation of ceramic materials. As was pointed out many years ago by von Mises[59] and by Taylor[60], for a fine grained polycrystalline solid to undergo plastic deformation each of the individual grains must be capable of a perfectly general change in shape. To satisfy this condition, each of the crystalline grains must possess five independent slip systems. If not, then voids are likely to develop

within the solids where the individual grains cannot conform to the change in shape of their neighbors. Groves and Kelly[61] have recently examined the observed crystallographic slip systems for a number of common ceramic materials to determine whether they allow the required general change in shape or not. Their results, reproduced in Table 1, are most interesting, they find that none of the common ceramic materials is capable of a great amount of plastic deformation at low temperatures (we shall discuss the high temperature case later).

TABLE I

THE NUMBER OF INDEPENDENT SLIP SYSTEMS FOR SOME COMMON CERAMIC CRYSTAL STRUCTURES

Structure	Crystallographic Slip Systems	Number of Independent Systems
NaCl (Low Temperatures) (eg. MgO)	$\{110\}\langle 1\bar{1}0\rangle$	2
NaCl (High Temperatures) (eg. MgO)	$\{110\}\langle 1\bar{1}0\rangle$ and $\{001\}\langle 1\bar{1}0\rangle$	5
Hexagonal (eg. Graphite, Al_2O_3)	$\{0001\}\langle 11\bar{2}0\rangle$	2
CsCl	$\{100\}\langle 010\rangle$	3
CaF_2 (Low Temperatures) (eg. UO_2)	$\{001\}\langle 110\rangle$	3
CaF_2 (High Temperatures)	$\{001\}\langle 1\bar{1}0\rangle$ and $\{110\}\langle 1\bar{1}0\rangle$	5
TiO_2	$\{101\}\langle 10\bar{1}\rangle$ and $\{110\}\langle 001\rangle$	4

One of the consequences of this failure to satisfy the von Mises criterion is demonstrated by the marked effect of grain size on the plastic properties of ionic solids at low temperatures. Figure 10 reproduces stress strain curves obtained on polycrystalline sodium chloride at room temperature[62]. As can be seen, decreasing the grain size has a comparatively small effect on the proportional limit, but a very large effect on the rate of work hardening. By the time there are three to five grains in the cross-section, the rate of work hardening has increased tenfold over that of the cubic orientation single crystal and for the finest grain size tested (.035 mm) it has increased thirtyfold over the single crystal. Similar effects have been found in polycrystalline silver chloride[63] and lithium fluoride[64] at low temperatures.

These observations may be interpreted as follows:

(i) Since "grown in" sources are not completely immobilized in these ionic solids there are plenty of sources for slip over $\{110\}$ planes. The stress to start these dislocations moving is relatively insensitive to grain size. In fact the slight dependence of proportional limit noted in Figure 10 would probably disappear with the use of higher sensitivity microstrain techniques.

(ii) As slip propagates and the whole polycrystalline matrix attempts to deform plastically, constraints develop at the grain boundaries due to the fact that there are only two independent slip systems (Table 1). Consequently the material as a whole cannot deform plastically and hardens at a rate almost determined by the elastic constants.

(iii) As the stress increases the constraints can be relaxed somewhat by local slip on additional systems. In particular slip on $\{001\}\langle 1\bar{1}0\rangle$ has been observed in the vicinity of grain boundaries in polycrystalline lithium fluoride at room temperature, as shown in Figure 11. This additional slip permits the small amount of plastic deformation observed in the stress strain curves of

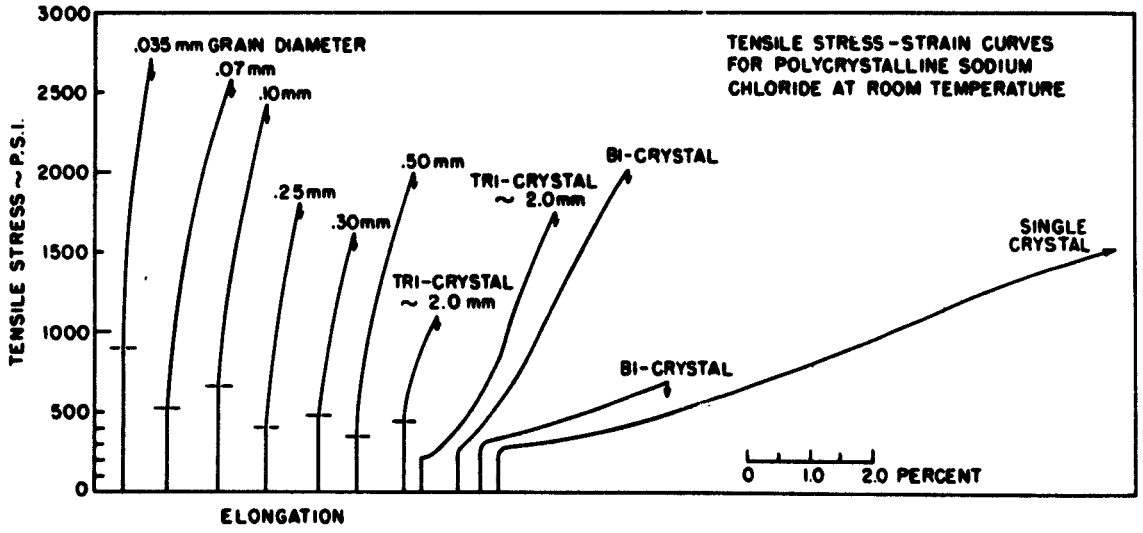

Figure 10 - Tensile stress strain curves for polycrystalline sodium chloride at room temperature illustrating the effect of decreasing the grain size on the proportional limit and rate of work hardening.

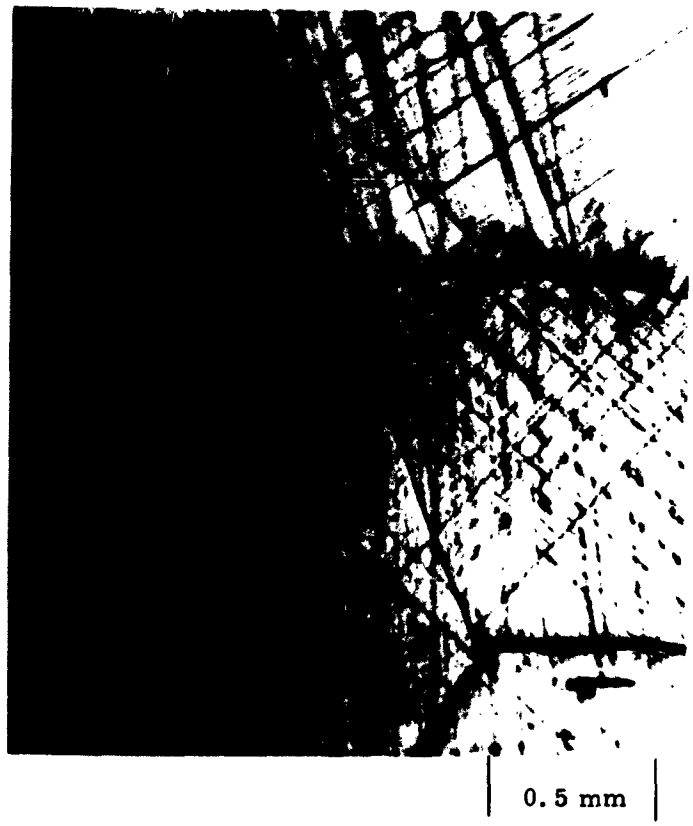

Figure 11 - Slip Distribution in the Vicinity of Grain Boundaries in Lithium Fluoride Deformed at Room Temperature. Note Very Local Slip on {001} Planes Near Triple Point. Slip Revealed by Etch Pit Technique. (Courtesy W. D. Scott and J. A. Pask).

Figure 10. Unfortunately the applied stress required to promote general slip throughout a grain on this $\{001\}\langle 1\bar{1}0\rangle$ system is far too high, for example in sodium chloride it is four times[65] and in lithium fluoride at least eight times[66] the stress to promote slip on the $\{110\}\langle 1\bar{1}0\rangle$ system at room temperature. Consequently the material as a whole cannot deform plastically by any great amount at least until the applied stress reaches this level.

(iv) The actual rate at which the stress increases, i.e., the rate of work hardening, is dependent on the grain size since the smaller the grain size the greater the grain boundary surface area and the greater the volume of constrained material wherein shear cannot take place. The exact relationship between grain size and the rate of work hardening under these conditions has neither been considered theoretically not determined experimentally.

The situation in magnesium oxide is even worse than in the simple halides. The stress to promote slip on the $\{001\}\langle 1\bar{1}0\rangle$ system at room temperature is approximately one hundred times higher than that to cause slip on the $\{110\}\langle 1\bar{1}0\rangle$ system[67] so that even local deformation of the kind illustrated in Figure 11 cannot be expected until extremely high stresses are reached. Thus, polycrystalline magnesium oxide shows virtually no plastic deformation at room temperature even though dislocations are quite mobile and the equivalent single crystals ductile. At higher temperatures the difference in stress level for slip on the two systems is reduced and at 1000° C is down to a factor of ten, equivalent to the situation in lithium fluoride at room temperature. A slight amount of plastic deformation has been observed in compression in this temperature range[67].

Again it must be emphasized that this discussion does not really apply to the low temperature mechanical behavior of ceramic materials in which dislocations are immobile (eg. Al_2O_3, TiO_2, TiC, etc., at room temperature).

In these materials the lattice resistance to dislocation motion is so high that the cohesive strength of the crystalline planes is exceeded before any plastic deformation is possible. The extent to which it may apply at high temperatures when these materials become plastic will be considered later in Section VI.

V. BRITTLE FRACTURE

In most of the preceding sections attention has been drawn to the plastic properties of ceramic materials, yet the fact remains that the most notorious mechanical property of a ceramic, particularly at low temperatures is its brittleness. The strength of a ceramic is always limited by brittle fracture. In this section we shall examine some of the aspects of brittle fracture in ceramics and shall show that in many instances the fracture strength can be related to the plastic properties described so far.

It is well known that the fracture strength of a brittle material falls far short of the theoretical strength (E/10) expected from simple estimates of interatomic forces. Equally familiar is the work of Griffith[68] who showed that the critical tensile stress (σ) to propagate a crack of length c is given by;

$$\sigma = \sqrt{\frac{E\gamma}{c}} \qquad (8)$$

where E is Young's modulus and γ the surface energy of the fractured faces. It is important to realize that equation (8) applies specifically to propagation in a purely elastic medium and assumes the pre-existence of cracks. It was for these reasons that Griffith was so successful in applying equation (8) to the strength of glass fibers, since, in glass, surface flaws are nucleated spontaneously by chemical reaction with the environment.

The nucleation, growth, and propagation of brittle fracture in crystalline solids is a vastly more complicated phenomenon. In the absence of pre-existing surface or internal defects a crack nucleus must be generated in some way and it has now been clearly demonstrated in a number of ceramic materials that crack nucleation can occur as a direct consequence of the limited amount of plastic deformation which precedes fracture[30, 69]. However, the

cracks nucleated by these various mechanisms are often too small to propagate catastrophically under the existing applied tensile stress and either the stress must increase or the cracks must grow to reach the critical dimension. Again it has been found that crack growth is assisted by local plastic deformation[70, 71]. When finally the crack reaches the critical dimension the condition for propagation is dictated by a modified form of the Griffith equation due to Orowan[72];

$$\sigma = \sqrt{\frac{E(\gamma + \gamma_p)}{c}} \qquad (9)$$

where γ_p represents the energy consumed by plastic deformation in the highly stressed region ahead of the propagating crack. This term γ_p is particularly important since its magnitude determines whether the solid is ultimately brittle or not. When γ_p is large a crack may be stalled for an indefinite period but when γ_p is small propagation may proceed without resistance. The value of γ_p is strongly dependent on the plastic properties of the solid. For most ceramic materials γ_p is inherently small and they are naturally brittle materials. Since not much can be done to remedy this latter situation most of the attention in ceramics has been focussed on the early stages of fracture. In particular fracture nucleation has been studied intensively and is probably the stage where improvements in the fracture characteristics are most likely to be implemented. Next, we shall discuss the role of structure and microstructure in the nucleation of brittle fracture in ceramics.

1. Crack Nucleation Due to Slip at Grain Boundaries

Crack nucleation has been studied most extensively in magnesium oxide. The essential feature is that cracks nucleate wherever groups of dislocations are obstructed either by other slip bands[73, 74] or by grain boundaries[75, 76, 77, 78]. The primary reason why these observations can be made so readily in magnesium oxide is that shear occurs at room temperature over flat {110} planar surfaces in discreet slip bands. Thus the deformation is distributed very inhomogeneously

and when a slip band is blocked by a microstructural barrier, such as a grain boundary, the stress concentration due to the dislocation pile up[79, 80] cannot be dissipated by secondary slip in the surrounding material. Instead a crack forms. Figure 12 shows a cleavage crack generated where a slip band intercepts the grain boundary in a magnesium oxide bicrystal under compression. Under tension such a cleavage crack switches into the intergranular surface and propagates immediately for fracture[78].

There are two possible ways to prevent the crack nucleation event recorded in Figure 12. Either slip within the grains should be made more homogeneous to relax the local stress concentration at the tip of the dislocation pile up or slip should be avoided altogether.

Efforts to make shear homogeneous have indeed resulted in a considerable improvement in the ductility of magnesium oxide single crystals[74] but similar attempts with bi-crystals and polycrystalline material have not been successful[78]. There are a number of reasons for this but the most general and important one for the present discussion arises from the fact that there are only two independent slip systems as indicated in Table 1[61]. Even when homogeneous slip does occur the high stresses developed in the boundary regions due to the incompatibility of the grains eventually exceeds the intergranular strength at certain points causing cracks to open up and the specimens to fracture. It is significant that the source of fracture under these conditions is always intergranular[62]. Thus in polycrystalline sodium chloride and lithium fluoride at room temperature, where slip is homogeneous and there is some measurable plastic deformation (see Figure 10) brittle fracture always originates from an intergranular source.

On the basis of these observations Stokes and Li[62, 78] concluded that the ability of magnesium oxide, or any other ceramic material for that matter, to slip at low temperatures is in fact an undesirable feature, and they have shown how the fracture strength of fully dense magnesia may be improved when steps are taken to eliminate slip.

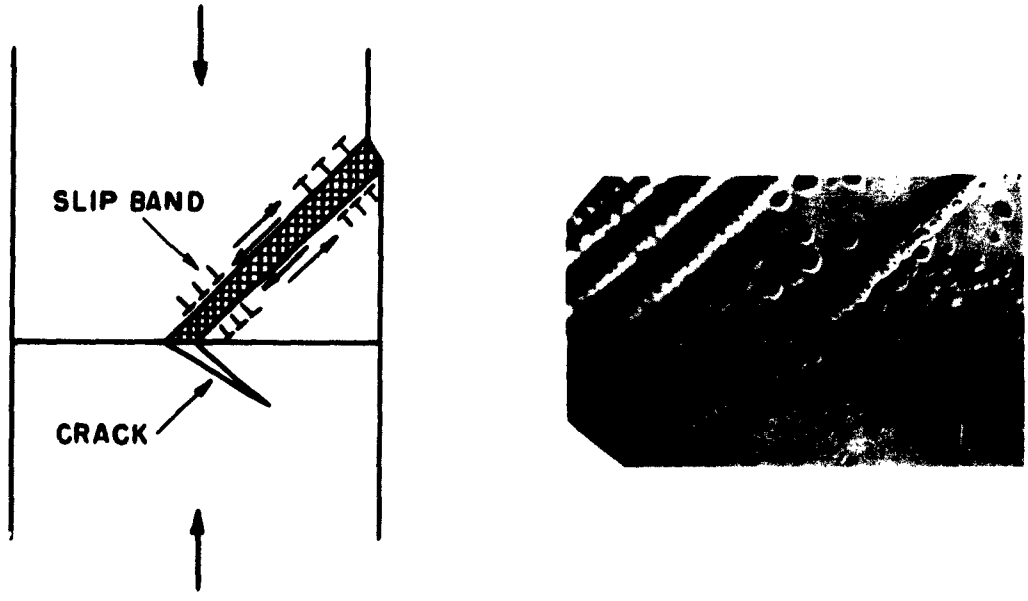

Figure 12 - Nucleation of a Cleavage Crack Due to Dislocation Pile Up at a Grain Boundary. Magnesium Oxide Bi-Crystal Deformed in Compression. Slip Revealed by Etch Pit Technique.

Table 2 summarizes recent results comparing the strength of polycrystalline magnesia in the presence and absence of active slip sources[78]. The tensile fracture strengths quoted in the right hand column represent the strength when "fresh" dislocation sources (introduced by the simple expedient of sprinkling the surface with fine silicon carbide powder[42]) are known to be present; the left hand column represents the strength when all possible precautions have been taken to remove surface dislocations by a chemical polish. It is instructive first to compare the fracture strength of bi-crystals with the yield strength of single crystals under the two extreme conditions discussed earlier in connection with dislocation locking (Section IV-1). The extremely high fracture strength of the bi-crystal obtained in the absence of slip (compare results 1 and 3) and the close agreement between the fracture strength and yield strength when slip sources are present (compare results 2 and 4) indicate that it is not the presence of the grain boundary per se but the interaction of slip with it which is responsible for the low fracture strength of the bi-crystal in result 4.

When similar care is taken to eliminate "fresh" dislocations from the surface of fully dense (100%) fine grained polycrystalline magnesia the tensile strength can be increased markedly, exceeding 30,000 psi in some cases. Again the average value (28,000 psi, result 5) for such specimens drops down to 18,500 psi when dislocations are reintroduced into the surface. It is believed that this remarkable surface sensitivity is due to the fact that fracture originates in these fully dense polycrystalline magnesia specimens by the slip dislocation mechanism of Figure 12.

Obviously this discussion of slip interaction with grain boundaries applies only to those solids in which dislocations can move easily at low temperatures. The extreme sensitivity to surface condition described in the previous paragraph is not likely to be found in materials such as alumina or rutile. The effect of surface damage on these materials will be discussed later.

TABLE 2

TENSILE STRENGTH OF MAGNESIUM OXIDE IN THE ABSENCE AND PRESENCE OF "FRESH" SURFACE DISLOCATIONS

Result	Material	Tensile Strength "Fresh" Dislocations ABSENT	Tensile Strength "Fresh" Dislocations PRESENT
1	Single Crystal	140,000 psi	
2	Single Crystal		10,000 psi
3	Bi-Crystal	110,000 psi	
4	Bi-Crystal		8,000 psi
5	Fully Dense (100%), As-received (Hot Pressed Polycrystalline (Grain size 20μ)	28,000 psi	
6	"		18,500 psi
7	Fully Dense (100%), Annealed, (Hot Pressed Polycrystalline (Grain size 75 μ)	19,500 psi	-
8	"		15,000 psi
9	99.7% Dense, As-received, Hot Pressed Polycrystalline (Grain size 30 μ)	12,000 psi	
10	"		9,000 psi
11	99.7% Dense, Annealed, Hot Pressed Polycrystalline (Grain size 50 μ)	11,500 psi	
12	"		12,500 psi

2. Effect of Porosity and Grain Size

When just a slight amount of porosity is present the magnitude of the difference in strength in Table 2 due to the presence or absence of surface dislocation sources is much less. For example, annealing the fully dense hot pressed material at 2000° C causes grain growth and the appearance of slight residual porosity in the grain boundary interface. The strength of polished material is then reduced to 19, 500 psi (result 7) and drops further only by one quarter (to 15, 000 psi, result 8) when surface dislocations are introduced[78]. In more conventional material of lower density (99. 7%) the tensile fracture strength is much lower (12, 000 psi) and the value is then apparently independent of surface treatment (results 9 through 12). These observations have been interpreted by assuming that the pores themselves provide stress concentrations which either initiate slip or nucleate intergranular failure directly. Thus, porosity in excess of 0. 1 to 0. 2 % tends to override any effects due to surface dislocations and the brittle fracture strength is more dependent on the amount and distribution of porosity.

It has long been realized that the strength of ceramics is sensitive to porosity and that the greatest changes occur following small departures from theoretical density. Ryshkewitch[81] and Duckworth[82] first demonstrated that the transverse bend strength (S), of alumina, zirconia, and silicate porcelain decreased exponentially with porosity as in equation (10);

$$S = S_o \exp(-bp) \qquad (10)$$

The form of this equation should be compared with equation (6). It is found experimentally that the value of k is generally one half the value found for b. A similar dependence has been established for thoria[83], uranium dioxide[84], and magnesia[85]. While the empirical relationship holds quite well when the

porosity exceeds 0.3%, for values less than this the strength is determined by other variables. In particular, equation (10) makes no allowance for the distribution and location of pores. It is to be expected that the stress concentration effect will depend critically upon whether the pores are interconnected (open) or isolated (closed) in any particular intergranular region at low porosity.

Similarly it is well known that decreasing the grain size increases the strength of a ceramic material. Knudsen[83] has suggested that the combined effects of grain size (d) and porosity (p) can be represented by equation (11);

$$S = S_o d^{-a} \exp(-bp) \qquad (11)$$

The value of a varies from 1/2 to 1/3 for a variety of materials and the equation has been found adequate to describe results for thoria[83], uranium dioxide[84], magnesia[85] and alumina[22, 85, 86] and for beryllium oxide[87] with a = 1.

Unfortunately most of this data on the transverse bend strength of ceramics as a function of grain size and porosity has been obtained on specimens of variable surface perfection. By surface perfection here we do not necessarily mean the presence or absence of surface dislocations considered earlier with respect to magnesia, but gross imperfections in the form of intergranular or cleavage ruptures generated by mechanical preparation techniques. Surface perfection is extremely important, for the presence or absence of flaws determines to a great extent the subsequent mechanical behavior and certainly contributes to the statistical nature of the strength of ceramics[88]. Harrison[89] has emphasized how surface flaws and damage introduced during grinding and lapping operations can lower the strength of polycrystalline magnesia. It follows that the empirical relationship of equation (11) may well represent the stress required to propagate existing surface defects through the microstructure rather than the stress to initiate cracks. In this case when a = 1/2, equation (11) corresponds to the Griffith equation (8) with the condition that c is related to the grain size d in some simple manner. In order to determine the effects of porosity and grain size systematically much more attention should be paid in the future to surface condition.

It is not easy to anticipate what the fracture strength dependence on grain size will be in the absence of surface flaws. Certainly it will depend on whether dislocations are mobile or not. When dislocations are mobile then the grain boundary interactions discussed in the previous section are important and the fracture strength dependence on grain size may follow a $d^{1/2}$ relationship of the type developed by Petch and Cottrell[90] for brittle metals. When dislocations cannot move, the fracture strength will be limited by internal stresses developed during firing and heat treatment. The internal stresses may be added to the applied stress and will be particularly severe in the boundary regions of anisotropic materials. All in all it seems reasonable to anticipate that the greatest low temperature fracture strengths will be obtained in materials of high density, fine grain size, perfect surface condition, in which dislocations cannot move. It is encouraging to note that transverse strengths in alumina in excess of 100,000 psi can be obtained under these conditions.

VI. HIGH TEMPERATURE DEFORMATION AND CREEP

At elevated temperatures, two factors become important to change the dependence of mechanical properties on microstructure. First, dislocations become more mobile on existing slip systems and new slip systems become possible, and second, the diffusion of point defects is enhanced to the point where they begin to contribute to the deformation.

1. Plastic Deformation and Ductile Fracture

The increased mobility of dislocations at high temperatures is reflected by a further drop in strength of single crystals of materials such as magnesium oxide[67] which are already plastic at low temperatures. It is also responsible for the onset of plasticity at reasonable stress levels in single crystals of materials like alumina[37, 38, 39], rutile[36, 91], and titanium carbide[92] which are not plastic at low temperatures. For the most part, these newly plastic ceramic materials slip on simple systems and the restrictions on polycrystalline ductility discussed earlier still apply.

The possibility of slip on multiple systems has more interesting consequences particularly for materials having the rock salt structure. As indicated in Table 1, slip becomes possible over $\{100\}$ planes in addition to the $\{110\}$ planes at high temperatures. The occurrence of $\{100\}$ slip contributes an additional three independent slip systems, making a total of five, thereby satisfying the condition for polycrystalline ductility. Stokes and Li[62] have shown that polycrystalline sodium chloride undergoes appreciable extension above 150° C, the temperature at which "wavy" or multiple slip is first observed. Under these conditions constraints do not develop in the grain boundary region and brittle fracture does not occur, instead the specimens extend continuously and neck right down to a point, giving a type of ductile fracture. The influence

VI. HIGH TEMPERATURE DEFORMATION AND CREEP

At elevated temperatures, two factors become important to change the dependence of mechanical properties on microstructure. First, dislocations become more mobile on existing slip systems and new slip systems become possible, and second, the diffusion of point defects is enhanced to the point where they begin to contribute to the deformation.

1. Plastic Deformation and Ductile Fracture

The increased mobility of dislocations at high temperatures is reflected by a further drop in strength of single crystals of materials such as magnesium oxide[67] which are already plastic at low temperatures. It is also responsible for the onset of plasticity at reasonable stress levels in single crystals of materials like alumina[37, 38, 39], rutile[36, 91], and titanium carbide[92] which are not plastic at low temperatures. For the most part, these newly plastic ceramic materials slip on simple systems and the restrictions on polycrystalline ductility discussed earlier still apply.

The possibility of slip on multiple systems has more interesting consequences particularly for materials having the rock salt structure. As indicated in Table 1, slip becomes possible over $\{100\}$ planes in addition to the $\{110\}$ planes at high temperatures. The occurrence of $\{100\}$ slip contributes an additional three independent slip systems, making a total of five, thereby satisfying the condition for polycrystalline ductility. Stokes and Li[62] have shown that polycrystalline sodium chloride undergoes appreciable extension above 150° C, the temperature at which "wavy" or multiple slip is first observed. Under these conditions constraints do not develop in the grain boundary region and brittle fracture does not occur, instead the specimens extend continuously and neck right down to a point, giving a type of ductile fracture. The influence

of grain size and porosity on ductile fracture has not been studied in sufficient detail yet to allow any conclusions to be drawn from the behavior of sodium chloride. However, similar work on silver chloride[63] in the temperature range where it exhibits wavy slip has shown that grain size has little or no effect on the rate of work hardening, again consistent with the fact that grain boundary constraints have been completely relaxed.

2. Creep and High Temperature Fracture

Unfortunately, the temperature range wherein a multiplicity of slip systems becomes available in most oxide ceramics is so high that additional complications come into play and the occurrence of plastic deformation by the simple movement of dislocations is never observed. Deformation at elevated temperatures is always enhanced by the diffusion of point defects and by the onset of viscous sliding at grain boundaries. The diffusion of vacancies or interstitial ions contributes to each of the three basic processes considered responsible for creep; dislocation climb, vacancy migration under stress, and grain boundary sliding. These will be described briefly in turn.

Dislocation climb occurs when vacant lattice sites condense on or escape from edge dislocations causing them to be displaced vertically in a direction perpendicular to the slip plane. The climb process permits unlike dislocations to move together and annihilate and it also permits dislocations to detour around obstacles in the slip plane. Thus, dislocations trapped in a pile-up against obstacles such as sub-grain or grain boundaries can escape by climb and rearrange themselves, the relaxation of the back stress enables the dislocation source to resume operation and deformation continues. When the rate of dispersion of the dislocations is approximately equal to the rate at which they are pumped into the pile-up a steady state creep rate is established. The rate controlling step in this process is vacancy diffusion, a fact which has been well-established for all metals for which accurate data is available[93]. In a detailed analysis of

the climb mechanism, Weertman[94] has shown that the creep rate ($\dot{\epsilon}$) varies with the applied stress (σ) and temperature (T) according to the following relationship;

$$\dot{\epsilon} \propto \sigma^{(9/2)} \quad \frac{\exp(-U/KT)}{T} \tag{12}$$

where U is generally the activation energy for self diffusion. In ceramics the presence of two ion species having different activation energies for self diffusion and the possibility that diffusion may occur in pairs makes the interpretation of U more difficult.

The remaining creep processes do not involve the motion of dislocations and apply specifically to polycrystalline material. In vacancy migration under stress, deformation results from diffusional flow within each crystal away from those boundaries where there is a high local compressive stress towards those boundaries having a high local tensile stress. This is generally referred to as Nabarro-Herring type creep and it has been estimated by these authors[95, 96] that the creep rate is related to the stress, temperature and grain size (d) by;

$$\dot{\epsilon} \propto \frac{\sigma D}{d^2 T} \tag{13}$$

where D is the diffusion coefficient and

$$d = D_o \exp(-U/KT) \tag{14}$$

It should be noted that the relationship for $\dot{\epsilon}$ in (13) differs from that in (12) by the power of the stress dependence and by the appearance of a grain size term. The linear relationship of $\dot{\epsilon}$ and σ in equation (13) gives rise to a viscous type of flow, at a rate determined by vacancy diffusion.

The exact mechanism of the third contributor to high temperature creep, grain boundary sliding, is not known. It has been shown that the shear strength of grain boundaries in ionic materials can fall off catastrophically at high temperatures[97, 98]. Whether this increased viscosity in the grain boundary region is due to the presence of an impure glassy phase or whether it is controlled by vacancy diffusion or dislocation motion through the disordered boundary region has not been determined. It is important to note that the creep rate due to this process is also roughly proportional to the applied stress but since it is dependent on the grain boundary surface area per unit volume it varies inversely as the grain size, i.e.,

$$\epsilon \propto \frac{\sigma}{d} \qquad (15)$$

Obviously, all three of these mechanisms occur together, to a certain extent, during high temperature creep. It is possible to distinguish which is the controlling mechanism by measuring the dependence of the creep rate on temperature, stress and grain size as may be appreciated by comparing equations (12) (13) and (15). This procedure is generally followed by workers in the field.

There is comparatively little systematic work on the effect of structure and microstructure on the creep of ceramics. Probably the earliest work on this subject is that by Wygant[99] who compared the creep rates of different ceramic materials. Data for materials of similar grain size or porosity at the same temperature and stress level are almost impossible to obtain, but Table 3, compiled by Kingery[4] gives some indication of the effect of crystal structure when most of these other variables have been fixed.

TABLE 3

COMPARISON OF TORSIONAL CREEP RATE FOR DIFFERENT POLYCRYSTALLINE CERAMIC MATERIALS

Material	Creep Rate at 1300° C 1800 psi (in/in/hr.)
Al_2O_3	0.13×10^{-5}
ZrO_2	3.0×10^{-5}
MgO (hydrostatic pressed, 2% Porosity)	3.3×10^{-5}
MgO (slip cast, 12% porosity)	33.0×10^{-5}
BeO	30.0×10^{-5}
ThO_2	100.0×10^{-5}

The most detailed studies of the effect of microstructure have been conducted on alumina, although even here the agreement amongst workers is varied. Tests have been performed on materials of different purity, porosity and grain size with different methods of loading. However, an attempt to interpret the results in a logical manner will be made with the help of Table 4. First, we compare the work of Rogers et al[100] and Kronberg[39] on single crystals in the temperature range 900-1700° C, (results 1 and 2 in Table 4). Although these tests were performed under different loading conditions, the activation energy for flow in both cases is approximately the same, 85 Kcal/mole. Since in Kronberg's tests the specimens were known to be deforming by simple slip on the basal plane, this may be regarded as the activation energy to initiate dislocation motion, i.e., to operate the synchro-shear mechanism[33] in single crystals.

TABLE 4

HIGH TEMPERATURE DEFORMATION AND CREEP OF SINGLE AND POLYCRYSTALLINE ALUMINA

Result No.	Material	Temperature Range	Rate Controlling Deformation Mechanism	Activation Energy Kcal/mole	Author
1	Single Crystal	900-1300° C	Basal Slip	85	Rogers et al (100)
2	Single Crystal	1200-1700° C	Basal Slip	85	Kronberg(39)
3(a)	Single Crystal	1800° C	Dislocation Climb	180	Chang (101)
3(b)	Single Crystal plus 2% Cr_2O_3	1800° C	Dislocation Climb	180	Chang (101)
4	Polycrystalline Lucalox, High Density 5-15μ grain size	1600-1800° C	Vacancy Migration	130	Warshaw and Norton (102)
5	Polycrystalline Lucalox, High Density, 5-35 μ grain size	1600-1800° C	Vacancy Migration	130	Folweiler (103)
6	Polycrystalline 97% Density, 50-100 μ grain size	1600-1800° C	Grain Boundary Sliding	185	Warshaw and Norton (102)
7(a)	Polycrystalline High Density, 100μ grain size	1750-1900° C	Grain Boundary Sliding	280	Coble and Guerard (104)
7(b)	Same as 7(a), plus Cr_2O_3	1750-1900° C	Grain Boundary Sliding	280	Coble and Guerard (104)
8(a)	Polycrystalline	1400-1700° C	Vacancy Migration and Grain Boundary Sliding	200	Chang (19)
8(b)	Same as 8(a), plus 1% Cr_2O_3	1400-1700° C	Vacancy Migration and Grain Boundary Sliding	200	Chang (19)
8(c)	Same as 8(a), plus 0.25% La_2O_3	1400-1700° C	Vacancy Migration and Grain Boundary Sliding	200	Chang (19)

At higher temperatures (above 1800° C) Chang[101] found single crystals to exhibit steady state creep at a rate dependent upon stress to the power 4.5 as in equation (12), indicating that it was controlled by the dislocation climb mechanism (result 3). The activation energy, 180 Kcal/mole, for dislocation climb, compares fairly well with the activation energy for diffusion of either the aluminum or oxygen ion determined by other means. The steady state creep rate of the alumina crystals was reduced by four orders of magnitude with the addition of 2% Cr_2O_3 as shown in Figure 13, but the activation energy for the process remained unchanged. The interpretation here is that the impurity is restricting motion of the dislocations over the slip plane, but does not change the rate at which they can climb.

With the introduction of grain boundaries there is an increase in the creep rate and a change in the creep mechanism from one controlled by dislocation climb to vacancy migration under stress. Studies on high density, fine grained alumina (Lucalox) by Warshaw and Norton[102] and Folweiler[103] illustrate this point. Both find the creep rate to vary linearly with the stress between 1500° C and 1800° C and the activation energy has been measured to be 130 Kcal/mole (results 4 and 5). Similarly Chang[19] has also found a viscous behavior although with a higher activation energy (result 8) in this temperature range. Paladino and Coble[105] have taken these results and estimated the diffusion coefficients (D in equation (13)) using the exact form of the Nabarro-Herring[96] equation. They have then compared them with the self-diffusion coefficient for the aluminum ion determined by independent means. The excellent agreement illustrated in Figure 14 confirms that the Nabarro-Herring mechanism is operating and indicates that the diffusion of aluminum ions is the rate controlling process. A similar correlation has now been established between the beryllium ion diffusion coefficient and the creep diffusion coefficient for beryllia[105, 106], and between the magnesium ion diffusion coefficient and the creep diffusion coefficient for magnesia at low stresses[107].

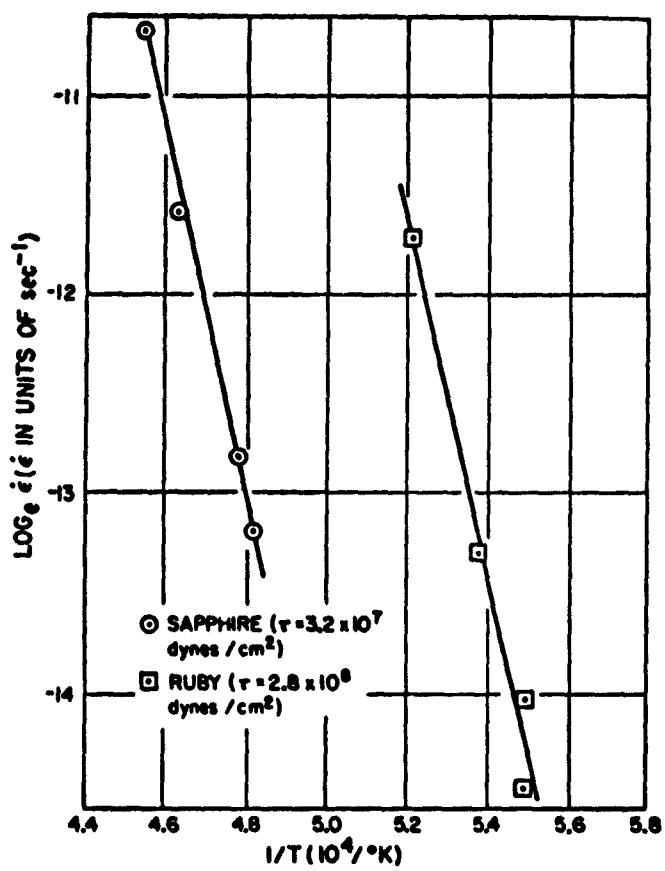

Figure 13 - Effect of purity on the steady state creep rate of alumina. The addition of 2% Cr_2O_3 lowers the creep rate by $\sim 10^4$. (After Chang[101]).

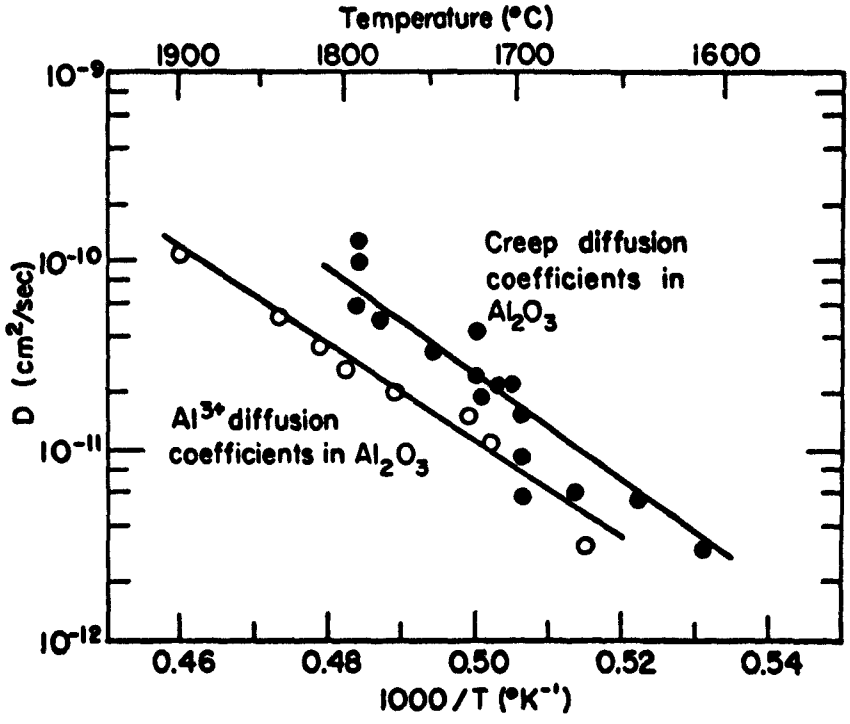

Figure 14 - Comparison of the diffusion coefficient measured for self diffusion of the aluminum ion with the diffusion coefficient calculated from creep data of alumina using the Nabarro-Herring equation. (After Paladino and Coble[105]).

Folweiler[103] studied the effect of grain size on the creep rate of Lucalox alumina and found a dependence inversely proportional to the square of the grain diameter, again consistent with the Nabarro-Herring theory as can be seen from equation (13). Thus, large grained material has a higher creep resistance than fine grained material.

At higher temperatures (1800° C-1900° C) and larger grain sizes the creep rate of alumina was found to increase at a rate more rapid than predicted by the vacancy migration theory (results 6 and 7). Warshaw and Norton[102] studied the stress dependence and found it to vary as the fourth power and on this basis suggested that a dislocation climb mechanism was rate controlling: however, in a more recent examination of this accelerated creep, Coble and Guerard[104] have suggested that grain boundary sliding has taken over. Their reasoning is based on the fact that an addition of Cr_2O_3 increases the creep rate even further; an observation also reported by Chang[19] for polycrystalline material (result 8). If dislocation climb is the controlling mechanism, then an addition of Cr_2O_3 should lower the creep rate as observed on alumina single crystals[101] and reproduced in Figure 13. If grain boundary sliding is the controlling mechanism then, as is known from anelasticity studies[19, 22] (Figure 6), the viscosity is lowered by the addition of impurities, and the creep rate should increase consistent with the experimental observations.

These observations on alumina may be summarized briefly as follows; single crystals creep by the dislocation climb mechanism and impurities lower the creep rate; polycrystals creep in the range 1200-1800° C by the migration of vacancies under a stress gradient and above 1800° C by grain boundary sliding, in both cases impurities raise the creep rate. There is a need for further experiments on bi-crystals to determine the stress dependence of grain boundary sliding and the effect of impurities on grain boundary viscosity.

Probably the reason why polycrystalline alumina creeps by the diffusion controlled mechanism rather than by dislocation climb is a consequence of the number of independent slip systems available. There are only two independent slip systems in alumina so long as basal slip predominates (Table 1) and, even taking into account the additional flexibility afforded by climb, polycrystalline material cannot deform by slip without the generation of intergranular constraints. The constraints can be relieved somewhat at high temperatures by the migration of vacancies but will eventually result in the appearance of intergranular voids in the regions of locally high tensile stress. Figure 15 shows the occurrence of grain boundary voids and sliding in polycrystalline alumina deformed at 1600° C. In magnesia, on the other hand, at a sufficiently high temperature and a high enough stress level, wavy slip occurs and recent tests in our laboratory[108] have shown that high density polycrystalline magnesia can be deformed substantially at 2000° C without the formation of intergranular voids. Under these conditions the creep rate might be determined by dislocation climb although this remains to be confirmed. At lower stress levels or slightly lower temperatures, slip in magnesia remains confined to $\{1\bar{1}0\}$ planes and the two independent slip systems are not then sufficient for creep to proceed by slip alone. Coble[107] has recently shown that under these conditions creep is controlled by vacancy migration under stress, although whether intergranular voids then open up remains to be determined. Certainly the high temperature behavior of magnesia as a function of stress, temperature and microstructural variables is a subject for more systematic and detailed investigation. The fact that fully dense material deforms without intergranular separation may make it superior to alumina for certain high temperature applications.

An increase in creep rate with porosity has long been recognized. Wygant[99] showed that the creep rate of a 2% porosity hydrostatically pressed magnesia was approximately one-tenth the creep rate of a 12% porosity slip cast material as shown in Table 3. Coble and Kingery[109] studied the effect of porosity on the creep rate of sintered alumina up to almost 50% porosity; their results are reproduced in Figure 16.

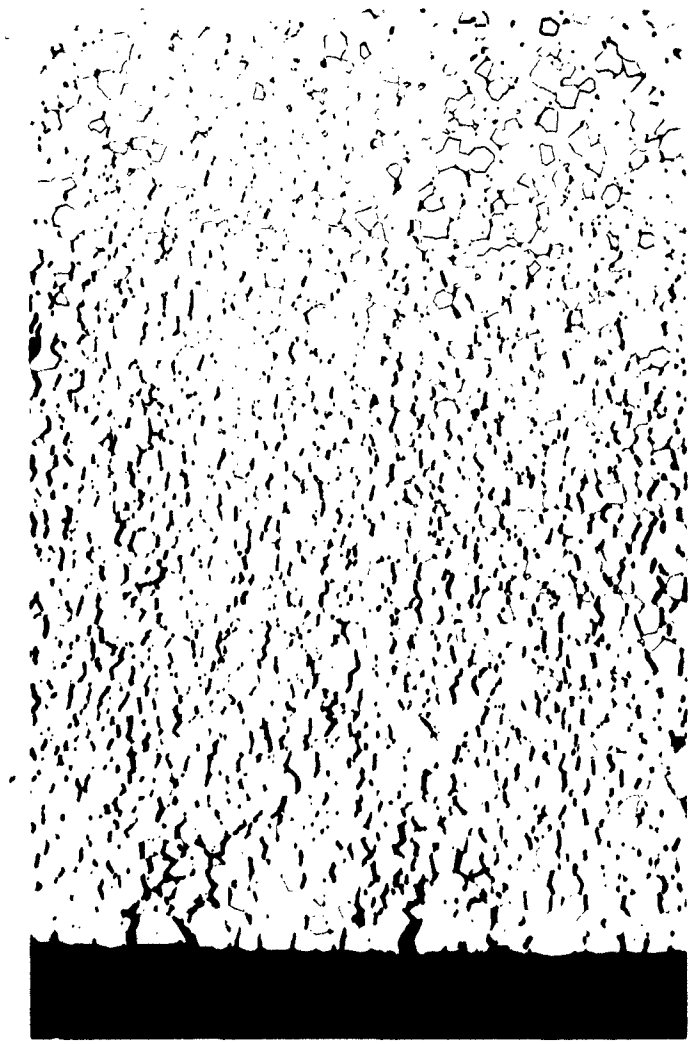

Figure 15 - Generation of Intergranular Voids During Torsional Creep of High Density Alumina. (Courtesy R. L. Coble).

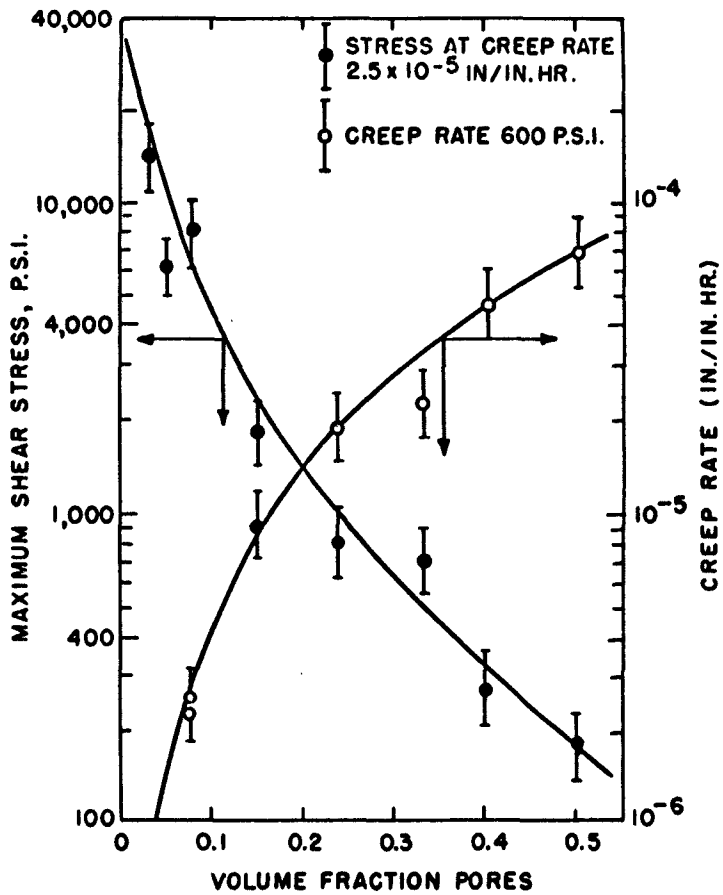

Figure 16 - Effect of porosity on the torsional creep of sintered alumina at 1275° C.

The stress to promote a constant creep rate and the creep rate at a constant stress are both plotted as a function of the porosity. (After Coble and Kingery[109]).

At temperatures where the deformation process is controlled by the migration of point defects, it is to be expected that stoichiometry will play an important role. Scott et al[110] showed that stoichiometric uranium dioxide (UO_2) could not be deformed until the temperature reached 1600° C, whereas a deviation in stoichiometry to $UO_{2.06}$ allowed plastic deformation around 800° C. The non-equilibrium cation vacancies are considered to contribute to creep at the lower temperatures. Similarly, Hirthe and Brittain[111] have shown that the activation energy for steady state creep in rutile changes gradually from 63 Kcal/mole at stoichiometric composition to 33 Kcal/mole for reduced material.

VII. CONCLUSIONS

This paper has attempted to correlate the mechanical properties of ceramics with fundamental microstructural variables. By necessity the discussion is limited to the simple alkali halide and pure oxide ceramics, but from this fundamental background it is to be hoped that a better appreciation of the mechanical behavior of more conventional ceramics can ultimately be attained. The salient points may be summarized as follows.

1) The maximum elastic modulus is obtained in material of highest density, in structures where the solid phase is continuous and the pores closed and spherical. The addition of a second phase of higher modulus causes the resultant modulus of the heterogeneous mixture to be increased.

2) The damping capacity of a ceramic single crystal at a particular temperature depends on the density and mobility of dislocations. The introduction of grain boundaries raises the damping capacity in a certain characteristic temperature range, this range can be broadened and extended to lower temperatures by the addition of impurity.

3) Ceramic materials deform plastically at the stress level and temperature at which dislocations are sufficiently mobile. The mobility of a dislocation can be reduced by impurities in a number of ways, (a) direct elastic interaction with impurity ions to lock the dislocation line, (b) indirect elastic interaction of the moving dislocation line with internal stress fields due to impurity ions in solid solution or precipitate particles, (c) electrostatic interaction of the dislocation line with charged point defects introduced to maintain neutrality. Each of these mechanisms leads to an increase in strength.

4) Plastic deformation of polycrystalline ceramics at low temperatures is prohibited by the lack of sufficient independent slip systems. At high temperatures some ceramic materials (eg. MgO) slip on additional systems and macroscopic polycrystalline ductility then becomes possible.

5) The tensile fracture strength at low temperatures is a maximum in fully dense, flaw free specimens of a ceramic material in which dislocations cannot move (eg. Al_2O_3). In the presence of porosity or surface damage the strength is determined by the critical stress to propagate a preexisting flaw. In the absence of porosity and surface damage brittle fracture occurs in those ceramics in which dislocations can move (eg. MgO) by the interaction of slip with grain boundaries, and in those ceramics in which dislocations cannot move the strength is limited by internal stresses developed in fabrication.

6) High temperature creep of ceramic single crystals occurs by dislocation motion and climb. Impurities hinder dislocation motion and thereby lower the creep rate of single crystals.

7) High temperature creep of polycrystalline ceramics generally occurs by vacancy migration under stress and grain boundary sliding. Impurities lower grain boundary viscosity and thereby increase the creep rate of polycrystals. Plastic deformation by dislocation motion and climb is generally restricted by lack of sufficient independent slip systems even at high temperatures.

Even with simple ceramic materials the above interpretations of mechanical behavior are still quite flexible and there remains a great need for critical theoretical and experimental work. Current developments of fully dense polycrystalline ceramics by novel fabrication techniques are providing the experimentalist with a good opportunity to perform quantitative experiments on well defined systems. The next few years should be particularly productive with respect to understanding the mechanical properties of polycrystalline material.

Acknowledgements

The author has benefited from discussions with colleagues at Honeywell Research Center, in particular the criticism of Dr. C. H. Li has been very helpful in arranging the material for presentation. I am grateful to Drs. G. W. Groves and A. Kelly and Professor R. L. Coble for making their manuscripts available before publication.

REFERENCES

1. R. L. Coble, Ceramic Fabrication Processes, M. I. T., and J. Wiley and Sons, Inc., New York (1958) p. 213.

2. J. J. Gilman and W. G. Johnston, Dislocations and Mechanical Properties of Crystals, J. Wiley and Sons, Inc., New York (1957) p. 116.

3. A. E. Gorum, E. R. Parker, and J. A. Pask, J. Am. Ceram. Soc., 41, 161 (1958).

4. W. K. Kingery, Introduction to Ceramics, J. Wiley and Sons, Inc., New York (1960) p. 597.

5. B. Paul, Trans. A. I. M. E., 218, 37 (1960).

6. Z. Hashin, J. Appl. Mechanics, 29, 143 (1962).

7. D. P. H. Hasselman and P. T. B. Shaffer, Factors Affecting Thermal Shock Resistance of Polyphase Ceramic Bodies, WADC Technical Report 60-749, Part II, April (1962).

8. C. Nishimatsui and J. Gurland, Trans. Am. Soc. Metals, 52, 469, (1960).

9. D. P. H. Hasselman, J. Am. Ceram. Soc., 46, 103 (1963).

10. J. K. Mackenzie, Proc. Phys. Soc. (London) (B), 63, 2 (1950).

11. R. L. Coble and W. D. Kingery, J. Am. Ceram. Soc., 39, 377 (1956).

12. P. Murray, D. T. Livey, and J. Williams, Ceramic Fabrication Processes, M. I. T. and J. Wiley and Sons, Inc., New York (1958) p. 147.

13. R. M. Spriggs, J. Am. Ceram. Soc., 44, 628 (1961).

14. F. P. Knudsen, J. Am. Ceram. Soc., 45, 94 (1962).

15. R. M. Spriggs, L. A. Brisette, and T. Vasilos, J. Am. Ceram. Soc., 45, 400 (1962).

16. D. P. H. Hasselman, J. Am. Ceram. Soc., 45, 452 (1962).

17. R. M. Spriggs and T. Vasilos, Paper presented at 63rd Annual Meeting, Am. Ceram. Soc., Abstract in Am. Ceram. Soc. Bull., 40, 187 (1961).

18. C. Zener, Elasticity and Anelasticity of Metals, University of Chicago Press, Chicago (1942).

19. R. Chang. J. Nuclear Materials, 1, 174 (1959).

20. J. B. Wachtman and L. H. Maxwell, WADC Technical Report 57-526 (1957).

21. J. E. Turnbaugh, Sc. D. Thesis, M. I. T. (1962).

22. W. B. Crandall, D. H. Chung, and T. J. Gray, Mechanical Properties of Engineering Ceramics, Interscience, New York (1961) p. 349

23. R. Chang. Mechanical Properties of Engineering Ceramics, Interscience, New York (1961), p. 209.

24. A. S. Nowick, Progress in Metal Physics, 4, 1 (1956). See also Acta Metallurgica, 10, 337 (1962).

25. R. B. Gordon and A. S. Nowick, Acta Metallurgica, 4, 514 (1956).

26. R. W. Whitworth, Phil. Mag., 5, 425 (1960).

27. A. Taylor, Acta Metallurgica, 10, 489 (1962).

28. P. Dahlberg, R. D. Carnahan, and J. D. Brittain, J. Appl. Phys., 33, 3493 (1962).

29. R. Chang, J. Appl. Phys., 32, 1127 (1961).

30. Mechanical Behavior of Crystalline Solids, Ceramic Educational Council Seminar, (1962), National Bureau of Standards Monograph 59 (1963).

31. J. J. Gilman, Acta Metallurgica, 7, 608 (1959).

32. W. A. Rachinger and A. H. Cottrell, Acta Metallurgica, 4, 109 (1956).

33. M. L. Kronberg, Acta Metallurgica, 5, 507 (1957).

34. S. Amelinckx and P. Delavignette, Mechanical Properties of Engineering Ceramics, Interscience, New York (1961) p. 105.

35. S. Amelinckx and P. Delavignette, Direct Observations of Imperfections in Crystals, Interscience, New York (1962) p. 295.

36. K. H. G. Ashbee and R. E. Smallman, J. Am. Ceram. Soc., 46, (1963).

37. J. B. Wachtman and L. H. Maxwell, J. Am. Ceram. Soc., 37, 291 (1954).

38. R. Scheuplein and P. Gibbs, J. Am. Ceram. Soc., 43, 458 (1960).

39. M. L. Kronberg, J. Am. Ceram. Soc., 45, 274 (1962).

40. W. G. Johnston and J. J. Gilman, J. Appl. Phys., 31, 632 (1960).

41. W. G. Johnston and J. J. Gilman, J. Appl. Phys., 30, 129 (1959).

42. R. J. Stokes, T. L. Johnston, and C. H. Li, Trans. A. I. M. E., 215, 437 (1959).

43. R. J. Stokes, Trans. A. I. M. E., 224, 1227 (1962).

44. J. D. Venables, Phys. Rev., 122, 1388 (1961).

45. J. D. Venables, J. Appl. Phys., 34, 293 (1963).

46. W. G. Johnston, J. Appl. Phys., 33, 2050 (1962).

47. W. J. Luhman and A. E. Gorum, Acta Metallurgica, 7, 685 (1959).

48. N. S. Stoloff, D. K. Lezius, and T. L. Johnston, J. Metals, 15, 84 (1963). J. Appl. Phys. (to be published).

49. R. J. Stokes and C. H. Li, Acta Metallurgica, 10, 535 (1962).

50. E. Schmid and W. Boas, Plasticity of Crystals, Hughes and Co., Ltd., London (1950) p. 236.

51. E. R. Parker, Mechanical Properties of Engineering Ceramics, Interscience, New York (1961) p. 65.

52. J. D. Eshelby, C. A. Newey, P. L. Pratt, and A. B. Lidiard, Phil. Mag., 3, 75 (1958).

53. P. L. Pratt, Symposium on Vacancies and Other Point Defects in Metals and Alloys, Institute of Metals, London (1957), p. 99.

54. A. E. Gorum, W. J. Luhman, and J. A. Pask, J. Am. Ceram. Soc., 43, 241 (1960).

55. J. E. May and M. L. Kronberg, J. Am. Ceram. Soc., 43, 525 (1960).

56. R. J. Stokes, Final Report on ASD Contract AF33(616)-7465, Nov. 1962.

57. F. G. Satkiewicz, Mechanical Properties of Engineering Ceramics, Interscience, New York (1961) p. 49.

58. T. S. Liu, R. J. Stokes, and C. H. Li, to be published.

59. R. von Mises, Zeit. Angew. Math. und Mech., 8, 161 (1928).

60. G. I. Taylor, J. Inst. Metals, 62, 307 (1938).

61. G. W. Groves and A. Kelly, Phil. Mag., to be published (1963).

62. R. J. Stckes and C. H. Li, Paper presented at Conference on Structure and Properties of Engineering Materials, Raleigh (1962), to be published.

63. R. D. Carnahan, T. L. Johnston, R. J. Stokes, and C. H. Li, Trans. A. I. M. E., 221, 45 (1961).

64. W. D. Scott and J. A. Pask, Paper presented at 64th Annual Meeting, Am. Ceram. Soc., Abstract in Am. Ceram. Soc. Bull., 41, 309 (1962).

65. S. Dommerich, Zeit. Fur Physik, 90, 189 (1934).

66. J. J. Gilman, Acta Metallurgica, 7, 608 (1959).

67. C. O. Hulse, S. M. Copley, and J. A. Pask, Paper presented at 65th Annual Meeting Am. Ceram. Soc., Abstract in Am. Ceram. Soc. Bull., 42, 187 (1963).

68. A. A. Griffith, Phil. Trans. Roy. Soc., (London) (A), 221, 163 (1921).

69. T. L. Johnston, C. H. Li, and R. J. Stokes, Strengthening Mechanisms in Solids, American Society for Metals, Cleveland, Ohio (1962) p. 341.

70. F. J. P. Clarke, R. A. J. Sambell, and H. G. Tattersall, Phil, Mag., 7, 393 (1962).

71. R. J. Stokes and C. H. Li, Fracture of Solids, Interscience, New York (1963).

72. E. Orowan, Fatigue and Fracture of Metals, J. Wiley and Sons, Inc., New York (1952), p. 135.

73. R. J. Stokes, T. L. Johnston, and C. H. Li, Phil, Mag., 4, 920 (1959).

74. R. J. Stokes, T. L. Johnston, and C. H. Li, Phil, Mag., 6, 9 (1961).

75. A. R. C. Westwood, Phil, Mag., 6, 195 (1961).

76. T. L. Johnston, R. J. Stokes, and C. H. Li, Phil. Mag., 7, 23 (1962).

77. F. J. P. Clarke, R. A. J. Sambell, and H. G. Tattersall, Trans. Brit. Ceram. Soc., 61, 61 (1962).

78. R. J. Stokes and C. H. Li, J. Am. Ceram. Soc., to be published.

79. C. Zener, Fracturing of Metals, American Society for Metals, Cleveland, Ohio (1948) p. 3.

80. A. N. Stroh, Advances in Physics, 6, 418 (1957).

81. E. Ryshkewitch, J. Am. Ceram. Soc., 36, 65 (1953).

82. W. Duckworth, J. Am. Ceram. Soc., 36, 68 (1953).

83. F. P. Knudsen, J. Am. Ceram. Soc., 42, 376 (1959).

84. F. P. Knudsen, H. S. Parker, and M. D. Burdick, J. Am. Ceram. Soc., 43, 641 (1960).

85. R. M. Spriggs and T. Vasilos, J. Am. Ceram. Soc., 46, (1963).

86. I. B. Culter, J. Am. Ceram. Soc., 40, 20 (1957).

87. C. Hyde, J. F. Quirk, and W. H. Duckworth, Quoted in reference (22).

88. W. Weibull, Proc. Ingen. Vetenskaps. Acad. 151, 1 (1939).

89. W. B. Harrison, Paper presented at 64th Annual Meeting, Am. Ceram. Soc., see Am. Ceram. Soc. Bull., 41, 311 (1962). To be published.

90. Fracture, John Wiley and Sons, Inc., New York (1959).

91. W. M. Hirthe, N. R. Adsitt, and J. O. Brittain, Direct Observations of Imperfections in Crystals, Interscience, New York (1962), p. 135.

92. W. S. Williams and R. D. Schaal, J. Appl. Phys., 33, 955 (1962).

93. J. E. Dorn, Creep and Recovery, American Society for Metals, Cleveland Ohio, (1957) p. 255.

94. J. Weertman, J. Appl. Phys., 26, 1213 (1955): 28, 362 (1957).

95. F. R. N. Nabarro, Conference on Strength of Solids, The Physical Society, London, (1948) p. 75.

96. C. Herring, J. Appl. Phys. 21, 437 (1950).

97. M. A. Adams and G. T. Murray, J. Appl. Phys., 33, 2126 (1962).

98. G. T. Murray, J. Silgailis, A. J. Mountvala, Report on Air Force Contract AF33(616)-7961. Report No. ASD-TDR-62-225.

99. J. F. Wygant, J. Am. Ceram. Soc., 34, 374 (1951).

100. W. A. Rogers, G. S. Baker, and P. Gibbs, Mechanical Properties of Engineering Ceramics, Interscience, New York (1962) p. 303.

101. R. Chang, J. Appl. Phys., 31, 484 (1960).

102. S. I. Warshaw and F. H. Norton, J. Am. Ceram. Soc., 45, 479 (1962).

103. R. C. Folweiler, J. Appl. Phys., 32, 773 (1961).

104. R. L. Coble and Y. H. Guerard, J. Am. Ceram. Soc. (to be published).

105. A. E. Paladino and R. L. Coble, J. Am. Ceram. Soc., 46, 133 (1963).

106. R. R. Vandervoort and W. L. Barmore, J. Am. Ceram. Soc., 46, 180 (1963).

107. R. L. Coble, Private Communication.

108. R. B. Day and R. J. Stokes, to be published.

109. R. L. Coble and W. D. Kingery, J. Am. Ceram. Soc., 39, 377 (1956).

110. R. Scott, A. R. Hall, and J. Williams, J. Nuclear Materials, 1, 39 (1959).

111. W. M. Hirthe and J. O. Brittain, Paper presented at 64th Annual Meeting, Am. Ceram. Soc., see Am. Ceram. Soc. Bulletin 41, 311 (1962).

TECHNICAL REPORT
Distribution List
Nonr-2456(00) NR032-451

Organization	No. of Copies
Chief of Naval Research Department of the Navy Washington 25, D. C. Attention: Code 423	(2)
Commanding Officer Office of Naval Research Branch Office 346 Broadway New York 13, New York	(1)
Commanding Officer Office of Naval Research Branch Office 495 Summer Street Boston 10, Massachusetts	(1)
Commanding Officer Office of Naval Research Branch Office 86 E. Randolph Street Chicago 1, Illinois	(1)
Commanding Officer Office of Naval Research Branch Office 1030 E. Green Street Pasadena 1, California	(1)
Commanding Officer Office of Naval Research Branch Office 1000 Geary Street San Francisco 9, California	(1)
Assistant Naval Attache for Research Office of Naval Research Branch Office, London Navy 100, Box 39 F. P. O., N. Y., N. Y.	(10)
Director U. S. Naval Research Laboratory Washington 25, D. C. Attention: Technical Information Officer, Code 2000 : Code 2020 : Code 6200 : Code 6300 : Code 6100	(6) (1) (1) (2) (1)
Chief, Bureau of Naval Weapons Department of the Navy Washington 25, D. C. Attention: Code RRMA : Code RREN-6	(1) (1)
Commanding Officer U. S. Naval Air Material Center Philadelphia, Pensylvania Attention: Aeronautical Materials Laboratory	(1)
Picatinny Arsenal Box 31 Dover, N. J. Attention: Lt. Hecht	(1)
Commanding Officer U. S. Naval Ordnance Laboratory White Oaks, Maryland	(1)
Commanding Officer U. S. Naval Proving Ground Dahlgren, Virginia Attention: Laboratory Division	(1)
Chief, Bureau of Ships Department of the Navy Washington 25, D. C. Attention: Code 315 335 341 350 364	(1) (1) (1) (1) (1)

Distribution List (Cont.)

Organization	No. of Copies
Commanding Officer U.S. Naval Engineering Experiment Station Annapolis, Maryland Attention: Metals Laboratory	(1)
Materials Laboratory New York Naval Shipyard Brooklyn 1, New York Attention: Code 907	(1)
Chief, Bureau of Yards and Docks Department of the Navy Washington 25, D. C. Attention: Research and Standards Division	(1)
Commanding Officer David Taylor Model Basin Washington 7, D. C.	(1)
Post Graduate School U.S. Naval Academy Monterey, California Attention: Dept of Metallurgy	(1)
Office of Technical Services Department of Commerce Washington 25, D. C.	(1)
Commanding Officer U.S. Naval Ordnance Test Station Inyokern, California	(1)
Armed Services Technical Information Agency (ASTIA) Documents Service Center Arlington Hall Station Arlington, Va.	(5)
Commanding Officer Watertown Arsenal Watertown, Massachusetts Attention: Ordnance Materials Research Office : Laboratory Division	(1) (1)

Organization	No. of Copies
Commanding Officer Officer of Ordnance Research Box CM, Duke Station Duke University Durham, North Carolina Attention: Metallurgy Division	(1)
Commander Aeronautical Systems Division Wright-Patterson Air Force Base Dayton, Ohio Attention: Aeronautical Research Lab. (WCRRL)	(1)
: Materials Laboratory (WCRTL)	(1)
: (ASRCEM-1)	(1)
U.S. Air Force ARDC Office of Scientific Research Washington 25, D. C. Attention: Solid State Division (SRQB)	(1)
National Bureau of Standards Washington 25, D. C. Attention: Metallurgy Division	(1)
: Mineral Products Division	(1)
National Aeronautics Space Administration Lewis Flight Propulsion Laboratory Cleveland, Ohio Attention: Materials and Thermodynamics Division	(1)
U.S. Atomic Energy Commission Washington 25, D. C. Attention: Technical Library	(1)
U.S. Atomic Energy Commission Washington 25, D. C. Attention: Metals and Materials Branch	(1)
Division of Research : Eng. Develop. Branch, Division of Reactor Development.	(1)

Distribution List (Cont.)

Organization	No. of Copies
Argonne National Laboratory Library Services Dept. Report Section, Bldg 14-Room 14 9700 S. Cass Ave., Argonne, Ill.	(1)
Brookhaven National Laboratory Technical Information Division Upton, Long Island New York Attention: Research Library	(1)
Union Carbide Nuclear Co. Oak Ridge National Laboratory P. O. Box P Oak Ridge, Tennessee Attention: Metallurgy Division	(1)
: Solid State Physics Division	(1)
: Laboratory Records Dept.	(1)
Los Alamos Scientific Laboratory P. O. Box 1663 Los Alamos, New Mexico Attention: Report Librarian	(1)
General Electric Company P. O. Box 100 Richland, Washington Attention: Technical Information Division	(1)
Iowa State College P. O. Box 14A, Station A Ames, Iowa Attention: F. H. Spedding	(1)
Knolls Atomic Power Laboratory P. O. Box 1072 Schenectady, New York Attention: Document Librarian	(1)
U. S. Atomic Energy Commission New York Operations Office 70 Columbus Avenue New York 23, New York Attention: Document Custodian	(1)
Sandia Corporation Sandia Base Albuquerque, New Mexico Attention: Library	(1)
U. S. Atomic Energy Commission Technical Information Service Extension P. O. Box 62 Oak Ridge, Tennessee Attention: Reference Branch	(1)
University of California Radiation Laboratory Information Division Room 128, Building 50 Berkeley, California Attention: R. K. Wakerling	(1)
Bettis Plant U. S. Atomic Energy Commission Bettis Field P. O. Box 1468 Pittsburgh 30, Pennsylvania Attention: Mrs. Virginia Sternberg, Librarian	(1)
Commanding Officer and Director U. S. Naval Civil Engineering Laboratory Port Hueneme, California	(1)
Commanding Officer U. S. Naval Ordnance Underwater Station Newport, Rhode Island	(1)
U. S. Bureau of Mines Washington 25, D. C. Attention: Dr. E. T. Hayes	(1)
Defense Metals Information Center Battelle Memorial Institute 505 King Avenue Columbus, Ohio	(2)
Solid State Devices Branch Evans Signal Laboratory U. S. Army Signal Engineering Laboratories c/o Senior Navy Liaison Officer U. S. Navy Electronic Office Fort Monmouth, New Jersey	(1)

Distribution List (Cont.)

Organization	No. of Copies
U. S. Bureau of Mines P. O. Drawer B Boulder City, Nevada Attention: Electro-Metallurgical Div.	(1)
Commanding General U. S. Army Ordnance Arsenal, Frankford Philadelphia 37, Pennsylvania Attention: Mr. Harold Markus ORDBA-1320, 64-4	(1)
Prof. E. R. Parker Division of Mineral Technology University of California Berkeley 4, California	(1)
D. T. Bedsole, Manager, Technical Library Aerojet-General Corporation Sacramento, California	(1)
Dr. R. A. Lad National Advisory Committee for Aeronautics Lewis Flight Propulsion Laboratory Cleveland, Ohio	(1)
Prof. E. S. Machlin School of Mines Columbia University New York, New York	(1)
Dr. G. T. Murray Materials Research Corp. 47 Buena Vista Avenue Yonkers, New York	(1)
Prof. R. Smoluchowski School of Engineering Princeton University Princeton, New Jersey	(1)
Prof. P. Gibbs Department of Physics University of Utah Salt Lake City, Utah	(1)
Prof. F. H. Norton Department of Metallurgy Massachusetts Institute of Technology Cambridge 39, Massachusetts	(1)
Prof. J. J. Gilman Division of Engineering Brown University Provident, Rhode Island	(1)
Dr. R. G. Breckenridge National Carbon Research Laboratories P. O. Box 6116 Cleveland 1, Ohio	(1)
Dr. J. R. Low General Electric Research Laboratories P. O. Box 1088 Schenectady, New York	(1)
Prof. B. L. Averbach Department of Metallurgy Massachusetts Institute of Technology Cambridge 39, Massachusetts	(1)
Dr. O. L. Anderson Bell Telephone Laboratories Murray Hills, New Jersey	(1)
Prof. W. D. Kingery Department of Metallurgy Massachusetts Institute of Technology Cambridge 39, Massachusetts	(1)
Prof. D. S. Wood Department of Mechanical Engineering California Institute of Technology Pasadena, California	(1)

Distribution List (Cont.)

Organization	No. of Copies
Prof. T. S. Shevlin 303 Roberts Hall University of Washington Seattle 5, Washington	(1)
Dr. B. Post Polytechnic Institute of Brooklyn 99 Livingston Street Brooklyn, New York	(1)
Prof. G. C. Kuczynski University of Notre Dame Notre Dame, Indiana	(1)
Prof. W. H. Robinson Physics Department Carnegie Institute of Technology Pittsburgh, Pennsylvania	(1)
Prof. R. Roy Department of Geophysics Pennsylvania State University University Park, Pennsylvania	(1)
Dr. F. A. Halden Department of Chemistry Stanford Research Institute Menlo Park, California	(1)
Prof. D. H. Whitmore Department of Metallurgy Northwestern University Evanston, Illinois	(1)
Prof. P. J. Bray Department of Physics Brown University Providence, Rhode Island	(1)
Prof. J. O. Brittain Northwestern University Evanston, Illinois	(1)
Prof. W. R. Buessem Department of Ceramic Technology Pennsylvania State University University Park, Pennsylvania	(1)
Prof. A. L. Friedberg Department of Ceramic Engineering University of Illinois Urbana, Illinois	(1)
Prof. P. L. Edwards Texas Christian University Fort Worth, Texas	(1)
Prof. I. B. Cutler University of Utah Salt Lake City, Utah	(1)
Dr. B. Phillips Tem-Pres Research, Inc. State College, Pennsylvania	(1)
Prof. J. B. Wagner, Jr. Northwestern University Department of Materials Science Evanston, Illinois	(1)
Prof. W. C. Hahn Department of Metallurgy Montana School of Mines Butte, Montana	(1)
Prof. S. R. Butler Physics Department University of New Hampshire Durham, New Hampshire	(1)
Prof. F. Seitz Department of Physics University of Illinois Urbana, Illinois	(1)
Prof. H. Brooks Dean of Graduate School of Applied Science Harvard University Cambridge, Massachusetts	(1)
Dr. LeRoy R. Furlong Bureau of Mines College Park, Maryland	(1)

Distribution List (Cont.)

Organization	No. of Copies
Prof. W. G. Lawrence New York State College of Ceramics Alfred University Alfred, New York	(1)
Prof. A. von Hippel Laboratory for Insulation Research Massachusetts Institute of Technology Cambridge 39, Massachusetts	(1)
H. R. Peiffer RIAS Inc. 7212 Bellona Avenue Baltimore 12, Maryland	(1)
Prof. J. Gurland Division of Engineering Brown University Providence, Rhode Island	(1)
Dr. J. T. Ransom Engineering Research Laboratory Experiment Station E. I. duPont and Co., Inc. Wilmington, Delaware	(1)
Dr. F. J. P. Clarke Metallurgy Division A. E. R. E. Harwell, Berkshire, England	(1)
Dr. R. Chang Atomics International P. O. Box 309 Canoga Park, California	(1)
Dr. I. Cadoff New York University University Heights New York, New York	(1)
Prof. F. V. Lenel Department of Metallurgical Engineering Rensselaer Polytechnic Institute Troy, New York	(1)
Prof. J.A. Pask Dept. of Mineral Technology University of California Berkeley 4, California	(1)
Prof. D. Turnbull Div. of Engineering and Applied Physics Pierce Hall Harvard University Cambridge 38, Massachusetts	(1)
Dr. J.B. Wachtman, Jr. National Bureau of Standards Division 9.6 Washington 25, D.C.	(1)
Dr. J.J. Duga Battelle Memorial Institute 505 King Avenue Columbus 1, Ohio	(1)
Dr. W.P. Shulof Dept. 32-26 AC Spark Plug Division Flint, Michigan	(1)
Dr. R.M. Spriggs Metals and Ceramics Research AVCO Corp. 201 Lowell Street Wilmington, Massachusetts	(1)